Mitigation of Silica Scaling by Closed-Circuit Reverse Osmosis

Stylianos Flambouris

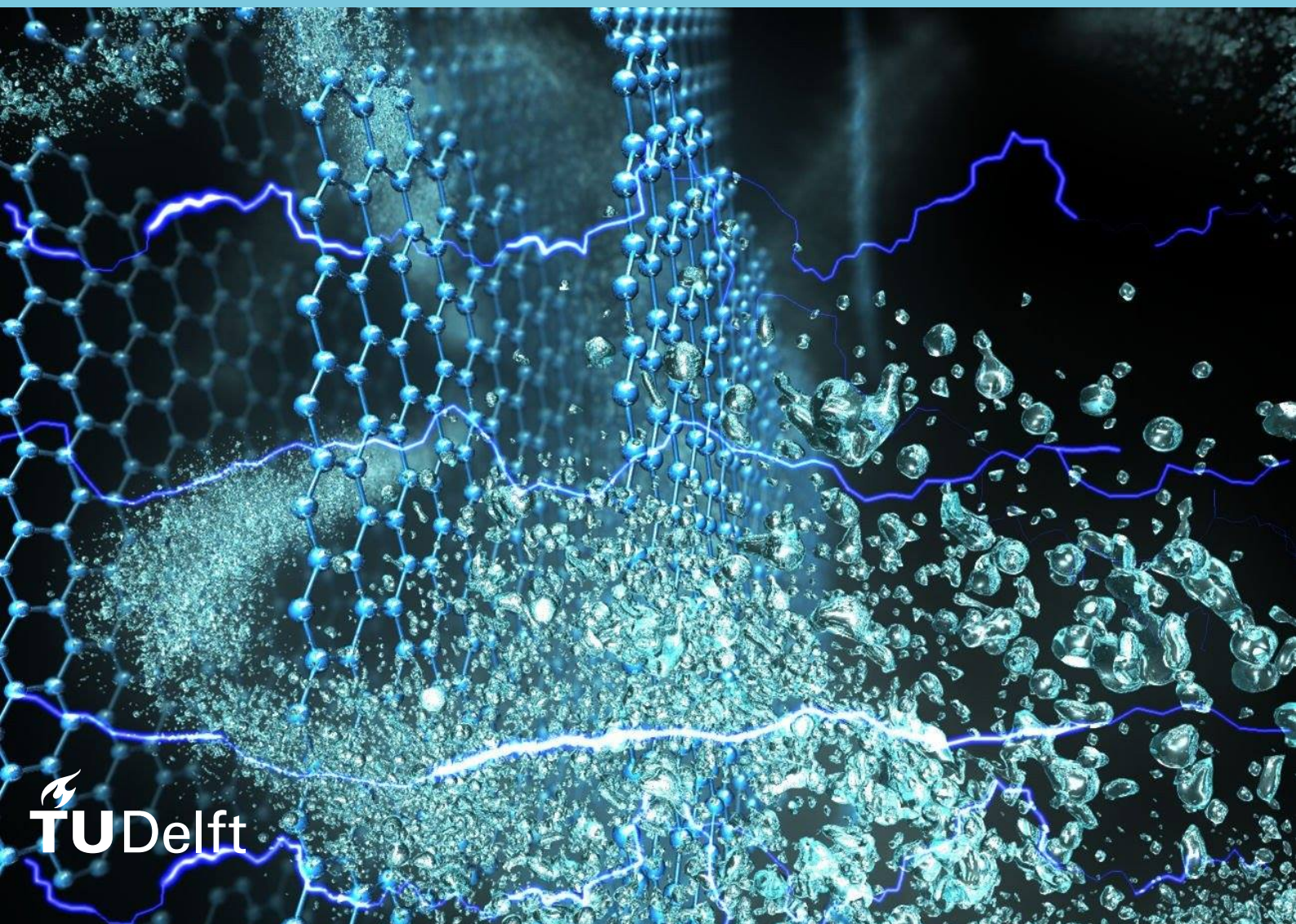

TU Delft

Mitigation of Silica Scaling by Closed-Circuit Reverse Osmosis

by

Stylianos Flambouris

to obtain the degree of Master of Science
at the Delft University of Technology,
to be defended publicly on Friday August 28, 2020 at 02:00 PM.

Student number:	4754301	
Project duration:	May, 2019 – August, 2020	
Thesis committee:	Dr. ir. S. G. J. Heijman,	TU Delft, chair
	Dr. ir. H. Spanjers,	TU Delft
	Prof. dr. E. J. R. Sudhölter,	TU Delft

This thesis is confidential and cannot be made public until August 28, 2022.

An electronic version of this thesis is available at `http://repository.tudelft.nl/`.

TU Delft Delft University of Technology

LENNTECH Water Treatment Solutions

Preface

The current master thesis constitutes the final act of my MSc program Environmental Engineering, at the Faculty of Civil Engineering and Geosciences at Delft University of Technology. I feel grateful because throughout this fruitful process I had the opportunity to gain invaluable experience and knowledge related to fascinating scientific topics and technologies as well as to face and overcome challenges of any kind.

At this point I would like to seize the opportunity and thank some people who, in one way or another, supported me during my thesis work. Of course, I would like to thank my supervisor, Bas Heijman, not only for his guidance and assistance on this specific project, but also for the overall cooperation we had on several occasions throughout my MSc studies. I would like also to thank Henri Spanjers and Ernst Sudhölter for their constructive feedback and remarks. Besides, I want to thank both of them, because Henri kindly accepted to join my assessment committee in midterm of the project, while Ernst was willing to continue being part of my committee despite his in-between retirement.

This study was carried out in collaboration with Lenntech B.V. I am very grateful to David van Lennep for giving me the opportunity to be part of the company as well as to work with the CCRO setup. I also owe a special thanks to my company supervisor, Rosario Gomes, for her willingness to support me as well as for getting me involved in some of the company's workshops and activities, during which I learned a lot about water treatment in practice. Timon van Oosten, thank you for your enthusiasm and your invaluable help when problems with my setup arose.

Furthermore, I would like to thank Armand Middeldorp for his support in the lab whenever this was needed as well as my colleagues and friends from Water Management and Environmental Engineering for their help and for creating a pleasant work environment. Finally, a special thanks goes to my family and friends for their tireless and vital support in every step of my life and career.

Stylianos Flambouris
Delft, August 2020

Abstract

Reverse osmosis (RO) is considered the most reliable and cost-effective membrane desalination technology worldwide. However, it suffers significant performance limitations due to mainly inorganic fouling generated in the highly concentrated brine. Especially, scaling caused by silica and silicates depositions results in irreversible damages with considerable economic implications. Recently, a different RO configuration, termed as closed-circuit reverse osmosis (CCRO), has been claimed to exhibit substantial benefits over conventional RO in terms of both energy savings as well as higher scaling resilience. CCRO is operated in batches, during which the generated brine is continuously recycled inside the closed loop until a desired recovery has been accomplished, after which the brine is released and replaced by fresh feed. Regarding CCRO scaling resistance superiority, an experimental-based proof is missing from the relevant literature. The current thesis was realized in collaboration with Lenntech B.V., aiming at investigating the intrinsic propensity of CCRO to withstand and delay silica scaling. To that end, a campaign of filtration tests was carried out by means of a single-module CCRO pilot setup, during which two scaling indicators were periodically monitored. The used indicators were the mass transfer coefficient (MTC) and the applied feed pressure (P_{feed}). Prior to the filtration trials, preliminary batch tests, of 4-hour duration each, were carried out in order to simulate and more thoroughly examine the circulated brine conditions. Various synthetic brines were prepared and silica polymerization was monitored. The effects of silica supersaturation level, pH and hardness ions were investigated. Of great importance was whether silica existed in its monomeric or polymeric form, since this greatly impacts the scaling occurrence probability. Batch tests results revealed that at high pH conditions (pH>10) monomeric silica concentration remained unchanged in pure silica solutions (even at high supersaturation levels), owing to the great silica solubility level. Nevertheless, when Mg^{2+} and/or Ca^{2+} were present in the solution, the quantity of silicic acid rapidly reduced. This was the result of the instantaneous formation of metal-silicate precipitates. Batch tests at pH 7 were also performed. In that case, monomeric silica concentration in pure silica solutions remained constant up to initial concentrations of about 450 mg/L SiO_2 for the examined 4-hour duration. However, at higher SiO_2 concentrations, such as at 750 mg/L, rapid polymerization occurred. When hardness cations were included in the neutral pH solutions, they showed an accelerating effect on silica polymerization process, but they did not react with either monomeric or polymeric silica. This effect relates to the suppression of the silica colloids diffuse double layer by the hardness cations, which subsequently facilitates colloids agglomeration. Regarding the CCRO filtration tests, they were conducted in sequences with duration of 20 or 40 min, which in its turn determined the achieved sequence recovery. For most of the carried out sequences the initial feed composition was: 120 mg/L SiO_2 and 24 mg/L Mg^{2+}. Only the final 5 out of the total 40 sequences were realized in the absence of magnesium in the feed solution. All the filtration runs were performed at pH 7, at ambient temperature and at constant flux 15 L/m^2h. The outcome was a scaling-free desalination process for a total cumulative operational period of approximately 11 hours, during which recoveries as high as 90.9% were reached, whereas severe scaling took place only after about 14 hours of total operation. The obtained results were contrasted with filtration tests results of conventional RO received from literature resources and in that way the higher efficiency of CCRO to withstand and delay silica scaling was proved. Additionally, through silica mass balance calculations it was shown that during all filtration tests significant silica polymerization took place. Also, cations analysis be means of IC excluded the participation of Mg^{2+} ions in the formed scale layer. It was concluded that the scale development was the result of an initial attachment of silica colloids to the membrane surface followed by monomeric units adsorption onto them. Finally, a simple customized method for the prediction of silica scaling potential in CCRO operations based on batch tests was proposed.

Contents

List of Figures ix

List of Tables xi

Nomenclature xiii

Acronyms xv

Glossary xvii

1 Introduction 1
1.1 General introduction . . . 1
1.2 Thesis motivation and scope . . . 2

2 Theoretical background 5
2.1 Closed-circuit reverse osmosis (CCRO) . . . 5
2.1.1 CCRO in comparison to conventional RO . . . 7
2.2 Silica aqueous chemistry . . . 8
2.2.1 Silica in natural waters and silica speciation . . . 8
2.2.2 Factors affecting silica speciation and solubility . . . 9
2.2.3 Silica scaling in RO systems . . . 11
2.3 Scaling detection and mass transfer coefficient (MTC) . . . 12

3 Materials and methods 15
3.1 Batch experiments . . . 15
3.2 CCRO experimental process . . . 16
3.2.1 Description of the CCRO setup . . . 16
3.2.2 Experimental procedure . . . 19
3.3 Conducted CCRO experiments . . . 20
3.3.1 Pristine membrane water permeability . . . 20
3.3.2 Concentration factor and recovery determination . . . 20
3.3.3 Scaling tests . . . 21
3.4 Chemical solutions . . . 22
3.5 Analytical methods . . . 22

4 Results 23
4.1 Batch tests results . . . 23
4.1.1 Pure silica solutions . . . 23
4.1.2 Silica/Ca^{2+} solutions . . . 24
4.1.3 Silica/Mg^{2+} solutions . . . 24
4.1.4 Silica/Ca^{2+}/Mg^{2+} solutions . . . 25
4.1.5 Effect of neutral pH . . . 26
4.1.6 Overview of the batch tests results . . . 28
4.2 Preliminary filtration tests . . . 29
4.2.1 Pristine membrane water permeability . . . 29
4.2.2 Recovery determination over time . . . 30
4.3 CCRO scaling tests . . . 31
4.3.1 CCRO scaling tests: 20 min sequence time . . . 31
4.3.2 CCRO scaling tests: 40 min sequence time . . . 32
4.3.3 Soluble silica mass balance . . . 35
4.3.4 Magnesium cations mass balance . . . 37
4.3.5 Overview of the filtration tests results . . . 38

5 Discussion **41**
5.1 Discussion on the batch tests results 41
5.2 Discussion on the CCRO filtration tests results 42
5.3 Overall discussion 45

6 Conclusions **47**

7 Recommendations **49**

A Composition of the batch solutions **55**

B Membrane specification data sheet **57**

C Composition of the CCRO feed solutions **59**

D Original graph from literature **61**

E Silica mass balance graphs **63**
E.1 SiO_2 mass balance for the 20 min sequences 6-10 63
E.2 SiO_2 mass balance for the 40 min sequences 1-5 63
E.3 SiO_2 mass balance for the 40 min sequences 11-15 64
E.4 SiO_2 mass balance for the 40 min sequences 21-25 64
E.5 SiO_2 mass balance for the 40 min sequences 26-30 65
E.6 Mg^{2+} mass balance for the 40 min sequences 16-20 65

List of Figures

2.1 Representation of a typical CCRO system [16]. 5
2.2 Alternation between the CCD/PFD modes [17]. 6
2.3 Silica reversible dissolution mechanism [21]. 9
2.4 Amorphous silica solubility dependence on pH and temperature assuming no other salts are present in solution [21]. 10
2.5 Formation reactions leading to silica and common metal silicates [25]. 10

3.1 Front and back view of the experimental setup provided by Lenntech B.V. 17
3.2 Schematic overview of the CCRO experimental setup. 17
3.3 Operational protocol of the entire experimental process. 20

4.1 Soluble silica concentration over time in the various tested batches. In the legend the initial SiO_2 concentrations of each batch solution are given. 23
4.2 Soluble silica concentration over time in the presence of Ca^{2+} cations. 24
4.3 Soluble silica and Ca^{2+} concentrations over time for a particular batch test. 25
4.4 Soluble silica and Mg^{2+} concentrations over batch time. The Mg^{2+} concentration variation (red curve) refers to the batch with initial silica 350 mg/L. 25
4.5 Soluble silica, Ca^{2+} and Mg^{2+} concentrations over batch time. The black dashed curve refers to a pure silica solution, whereas the three solid curves refer to the same solution with the quantity of each constituent indicated in the legend. 26
4.6 Soluble silica concentration over batch time at pH 7 (dashed curves) and at pH > 10 (solid curve). The data regarding pH 7 runs were received from [4]. 27
4.7 Soluble silica concentration (blue curves) over experimental time at pH 7. The red curve corresponds to Mg^{2+} concentration over time in the solution with initial SiO_2 460 mg/L. . 27
4.8 Soluble silica and Ca^{2+} concentration variations over time at pH 7 for the solution with initial composition: SiO_2 460 mg/L and 260 mg/L Ca^{2+}. For comparison, silica concentration of the respective SiO_2/Mg^{2+} solution is also given. 28
4.9 Comparative graph of soluble silica concentrations over time for the various examined batches at pH above 10. In all batches the initial SiO_2 concentration was 350 mg/L. Whenever Ca^{2+} and/or Mg^{2+} were preset their concentration was 195 mg/L and 120 mg/L, respectively. 29
4.10 Comparative graph of soluble silica concentrations over time for the various examined batches at pH 7. In the SiO_2/Ca^{2+} solution the concentrations were 460 and 260 mg/L, respectively, whereas in the SiO_2/Mg^{2+} solution the concentrations were 460 and 160 mg/L, respectively. 29
4.11 Permeate flux as function of different applied TMPs. 30
4.12 Sulfate concentration in the recycled brine at different time points. 30
4.13 MTC and applied P_{feed} variations over time for sequences 1 - 5. Each sequence duration was 20 min. 32
4.14 MTC and applied P_{feed} variations over time for sequences 6 - 10. Each sequence duration was 20 min. 32
4.15 MTC and applied P_{feed} variations over time for sequences 1 - 5. Each sequence duration was 40 min. 33
4.16 MTC and applied P_{feed} variations over time for sequences 6 - 10. Each sequence duration was 40 min. 33
4.17 MTC and applied P_{feed} variations over time for sequences 11 - 15. Each sequence duration was 40 min. 34
4.18 MTC and applied P_{feed} variations over time for sequences 16 - 20. Each sequence duration was 40 min. 35

4.19 MTC and applied P_{feed} variations over time for sequences 21 - 25. Each sequence duration was 40 min. 35
4.20 MTC and applied P_{feed} variations over time for sequences 26 - 30. The feed solution contained 120 mg/L SiO_2 in the absence of Mg^{2+}. Each sequence duration was 40 min. 36
4.21 Measured and calculated soluble SiO_2 concentration values in the final brine of each 20 min sequence. The depicted values concern sequences 1 - 5. 36
4.22 Measured and calculated soluble SiO_2 concentration values in the final brine of each 40 min sequence. The depicted values concern sequences 6 - 10. 37
4.23 Measured and calculated soluble SiO_2 concentration values in the final brine of each 40 min sequence. The depicted values concern sequences 16 - 20. 37
4.24 Measured and calculated Mg^{2+} concentration values in the final brine of each 40 min sequence. The depicted values concern sequences 21 - 25. 38
4.25 Overview of the CCRO tests. The conducted CCD sequences have been placed consecutively over the cumulative CCD operational time. 39

5.1 Silica deposition mechanism under highly supersaturated conditions [44]. 43

B.1 Specification data sheet of the BW30-4040 membrane element used in the experimental process. 57

D.1 Soluble silica concentration variation over time in the absence of hardness ions at pH 7. The graph was received from [4]. 61

E.1 Measured and calculated soluble SiO_2 concentration values in the final brine of each 20 min sequence. The depicted values concern sequences 6 - 10. 63
E.2 Measured and calculated soluble SiO_2 concentration values in the final brine of each 40 min sequence. The depicted values concern sequences 1 - 5. 63
E.3 Measured and calculated soluble SiO_2 concentration values in the final brine of each 40 min sequence. The depicted values concern sequences 11 - 15. 64
E.4 Measured and calculated soluble SiO_2 concentration values in the final brine of each 40 min sequence. The depicted values concern sequences 21 - 25. 64
E.5 Measured and calculated soluble SiO_2 concentration values in the final brine of each 40 min sequence. The depicted values concern sequences 26 - 30, which were conducted in the absence of Mg^{2+}. 65
E.6 Measured and calculated Mg^{2+} concentration values in the final brine of each 40 min sequence. The depicted values concern sequences 16 - 20. 65

List of Tables

2.1 Overview of the various silica forms encountered in aqueous solutions. 9
2.2 Overview of the main factors affecting silica solubility. 11

3.1 Overview of the conducted batch tests. Single x indicates batches performed without pH adjustment, whereas double x batches performed both with and without pH adjustment. The initial concentration of each of Mg^{2+} and Ca^{2+} was 1 mM. 16
3.2 Description of the CCRO setup parts. 18
3.3 Membrane main features. 18

4.1 Concentration factors and recoveries versus elapsed times in the various trials. 31

A.1 Overview of the conducted batch tests. The values shown in the table represent the final concentrations of SiO_2 (theoretical initial value 70 or 120 mg/L), Mg^{2+} (theoretical initial value 24 mg/L) and Ca^{2+} (theoretical initial value 40 mg/L) used in the prepared batches after the indicated recovery (R) had been achieved. 55

C.1 The exact composition of the prepared feed solutions employed in the performed CCRO filtration experiments. 59

Nomenclature

Greek Symbols

Δ_π	Osmotic pressure difference	[Pa]
π_c	Osmotic pressure of the concentrate stream	[Pa]
π_f	Osmotic pressure of the feed stream	[Pa]
π_p	Osmotic pressure of the permeate stream	[Pa]
τ	Tortuosity	[-]

Latin Symbols

A_{mem}	Active surface area of the membrane	[m^2]
d_{pore}	Pore diameter	[m]
J_w	Permeate flux	[$m^3/m^2 s$]
K_w	Membrane water permeability	[m]
l	Membrane thickness	[m]
$MR(\%)$	Module recovery	[%]
MTC	Mass transfer coefficient	[m/s Pa]
N	Total number of cycles during a sequence	[-]
NDP	Net driving pressure	[Pa]
p	Porosity	[-]
P_c	Pressure of the concentrate stream	[Pa]
P_{feed}	Applied feed pressure	[Pa]
P_f	Pressure of the feed stream	[Pa]
P_p	Pressure of the permeate stream	[Pa]
Q_c	Flow rate of the concentrate during a PFD sequence	[m^3/s]
$Q_{f,fresh}$	Flow rate of the fresh feed	[m^3/s]
Q_p	Flow rate of the produced permeate	[m^3/s]
Q_{recirc}	Flow rate of the recirculated stream	[m^3/s]
$R(\%)$	Recovery	[%]
$R_{seq}(\%)$	Recovery achieved during a CCD sequence	[%]
$R_{sys}(\%)$	Total system recovery	[%]
T	Temperature	[^oC]
t_{cycle}	Cycle duration	[s]

t_{seq}	Sequence duration	[min]
TCF	Temperature correction factor	[-]
TMP	Trans-membrane pressure	[Pa]
$V_{f,fresh}$	Volume of the incoming fresh feed	[m^3]
V_p	Volume of the produced permeate	[m^3]
V_{sys}	System intrinsic volume	[m^3]

Acronyms

AFM Atomic Force Microscopy.

CCD Closed-Circuit Desalination.

CCRO Closed-Circuit Reverse Osmosis.

CF Concentration Factor.

CP Concentration Polarization.

EC Electrical Conductivity.

ERD Energy Recovery Device.

HPP High Pressure Pump.

IC Ion Chromatography.

PFD Plug Flow Desalination.

PUR Power-Up Rinse.

PV Pressure Vessel.

RO Reverse Osmosis.

SDF Shut Down Flush.

SEC Specific Energy Consumption.

SWRO Sea Water Reverse Osmosis.

TDS Total Dissolved Solids.

VFD Variable Frequency Drive.

Glossary

amorphous silica General term including any kind of silica lacking crystalline structure.

brine Highly saline concentrate stream produced as by-product during RO applications.

CCD sequence Operation mode during which the concentrate is recirculated inside the CCRO loop until a desired recovery is achieved. This is the actual desalination mode.

colloidal silica Tiny spherical particles formed after monomers polymerization. According to IUPAC, their sizes range between 0.001 and 1 μm.

crystalline silica Silica species displaying crystalline molecular structure. The most common type is quartz.

cycle A complete circulation of the water through the entire CCRO system.

monomeric silica Also called reactive and soluble silica or monosilicic and silicic acid. Most commonly, it comprises the dissolved form of silica and it is described by the chemical formula $Si(OH)_4$.

nucleation induction time Period between supersaturation achievement and the formation of stable crystals.

particulate silica Small particles formed after colloids agglomeration. They can be separated from the solution by means of a 0.45 μm filter.

permeate Pure water produced after the desalination process of a feed stream during RO applications.

PFD sequence Operation mode during which concentrate is released and not recirculated inside the CCRO loop. This mode serves for the system flushing.

polymeric silica Also called polysilicic acid. It contains two or more than two silicon atoms and it is formed after the bonding of monomeric units through dehydration reactions.

polymerization Process during which monomeric units react with each other to form larger polymers.

semi-batch RO Process during which fresh feed is continuously introduced in the system replenishing the produced permeate exiting the system.

silanol The functional group Si-OH often encountered in silica chemistry.

silica Material family including a wide range of species described by the chemical formula SiO_2. In nature, it is most commonly encountered as quartz.

silicon Metalloid chemical element with the symbol Si.

1 Introduction

1.1. General introduction

Current global challenges such as the ever increasing population growth along with the climate change intensification have seriously jeopardized the hitherto reliable fresh water resources. Therefore, the need to turn into alternative water sources (like saline and brackish) has become more urgent than ever. Since the purification of saline water constitutes a prerequisite prior to its exploitation in domestic and industrial applications, desalination processes have inevitably come to the fore over the last decades. Among the available desalination technologies, reverse osmosis (RO) has proven to be the most reliable as well as cost-effective one and therefore it is nowadays the most widely applied option [1]. RO comprises a pressure driven membrane technology, capable of removing even monovalent ions from an aqueous solution and producing pure water, termed as the permeate. Nevertheless, despite its wide employment and its relative superiority over other concentration-, electrical potential- or thermal-based desalination technologies, RO demonstrates two major issues related to high energy demands on the one hand and to the wastage of an important amount of feed water on the other [2]. In RO applications the wasted feed water, called the brine, comprises the highly concentrated stream which remains in the feed side of the membrane after the permeate extraction and which should appropriately be disposed of. Currently, conventional methods of brine disposal involve its direct release into ocean bodies or evaporation ponds as well as its injection into the deep subsoil [3]. However, due to important legal, environmental and economic constraints, the suitable disposal strategy often constitutes a major challenge for plant operators, especially in the case of inland desalination facilities. Therefore, minimization of the generated brine volume is always desirable, which technically corresponds to the maximum achievable recovery as possible. On the other hand, higher recovery also translates into a more concentrated waste stream and thus into a greater concentration polarization effect, rendering membranes vulnerable to scaling, particularly the tail elements of RO installations which experience supersaturated conditions on a continuous basis. Under those highly saline circumstances, the solubility product of various sparingly soluble salts, such as $CaCO_3$, $CaSO_4$ and silica, may be exceeded increasing the probability of precipitates formation. The occurrence of scaling has a clear adverse effect on membrane performance, as it enhances its resistance to the permeate passage causing permeate flux reduction. Consequently, higher energy consumption is required by the high pressure pump in order to maintain constant flux. Besides, scale formation induces recurring operation shutdowns, dedicated to chemical and mechanical cleanings, whereas in many cases frequent membrane replacements are inevitable [4].

Over the last decades, significant progress regarding RO membranes performance has been made. More specifically, the energy demand related to RO operations has been considerably decreased. Indicatively, it is noted that the energy consumption for sea water reverse osmosis (SWRO) has been dropped from 10 – 15 kWh/m^3 to approximately 2 kWh/m^3 over the last 50 years [5]. The reason behind this important advancement lies in both the improvements of the membrane materials themselves as well as in the introduction of energy recovery devices (ERD), which allow for partial recovery of the energy entailed in the pressurized brine [3]. However, despite the aforementioned amelioration concerning energy requirements, RO installations continue to suffer great performance limitations owing

to the risk of scaling. Silica in particular, comprises a persistent and hard to tackle precipitant due to its non-reactivity with usual cleaning acids. Therefore, it has been common practice for water treatment facilities to operate RO systems at relatively low recoveries in order to prevent scaling. This strategy, however, leads to substantial water wastage and produces large brine volumes, the treatment of which frequently constitutes a complicated task.

According to a recent study conducted by Werber et al. [6], significant additional improvement regarding RO efficiency is not expected to emerge from further modifications related to membrane materials, but rather from the optimization of the RO process itself. In recent years, research has been focused on innovative RO configurations, namely batch and semi-batch processes, which appear to display considerable advantages over traditional RO systems [7]. Closed-circuit reverse osmosis (CCRO) constitutes such a semi-batch system, in which the concentrate is recirculated inside the loop and it is only discharged when a specific predefined system recovery has been reached [8]. Although still in a relatively premature stage, as far as its broad full scale implementation is concerned, CCRO has attracted great scientific interest and already several studies' results have highlighted its potentially enhanced desalination efficacy in comparison to conventional RO. More specifically, two independent research groups from the U.S. [9, 10], based on numerical modeling predictions, compared CCRO with conventional RO systems in terms of energy consumption and presented quantitative evidence of substantial energy savings when the CCRO configuration was applied, especially at high recovery grades. Similar conclusions, in favor of CCRO, were drawn by Qiu and Davies [11], who mathematically estimated the theoretical limits of the normalized specific energy consumption (SEC) for different RO configurations. Furthermore, in his article Stover [12] employed real data from commercial inland installations treating brackish water to support CCRO superiority over conventional RO. Although in this work CCRO was described as fouling resilient, main focus of the study was to establish it as a low energy-intensive configuration. Another research more dedicated to scaling investigation was conducted by Efraty [8], who used the IMS Design software to simulate the treatment of a brine (>10000 ppm) containing high initial silica concentration (>124 ppm) by a single-module CCRO system. The outcome could be considered as promising, since when proper antiscalant and low pH (3 - 5) were applied the brine was effectively treated up to 83% recovery, without warning statements from the projection software. The transition from theoretical model simulations to experimental trials was realized by the studies of Gal et al. [13] and Sonera et al. [14], during which actual CCRO pilot experiments were carried out. In the former case, municipal water (553 μS/cm) containing 32 ppm of silica was processed reaching a high recovery of 96%, whereas in the latter well water with 57 ppm of silica was treated (TDS: 1304 mg/L) up to a 93.8% recovery. The applied operational pH values were 5 and 5.5, respectively, whereas appropriate antiscalants were used. In both cases, the results revealed a high efficacy of the CCRO configurations to treat various feed waters under supersaturated conditions, since in neither trial fouling and/or scaling indications were shown. More recently, various pure silica solutions having initial concentrations ranging from 70 to 120 mg/L were treated by a CCRO system as part of a study conducted at TU Delft investigating silica scaling [15]. In those experiments, as high recovery as 93% was achieved without silica fouling occurrence, under alkaline conditions (pH>10) and without usage of antiscalants.

1.2. Thesis motivation and scope

Previous studies investigating CCRO performance have revealed a promising potential of this technology in terms of energy savings as well as of resilience to scaling. Regarding the latter, however, there are only limited studies that performed pilot-scale experiments to investigate scaling and hardly any studies that have focused on the contribution of the CCRO configuration itself. That is to say, the conducted filtration tests were carried out under conditions that hamper scaling development (e.g. usage of dedicated antiscalants, low pH), thus the effect of this particular configuration could not be isolated and easily examined. Additionally, silica comprises a very persistent scalant causing several issues during RO applications as well as the exact mechanisms related to silica scaling are not well-understood yet.

The current study aims to evaluate the effectiveness of CCRO in resisting and retarding silica scaling as well as to identify important factors that have an effect on the scaling process. To that end, pilot-scale CCRO filtration tests were carried out treating feed water containing high silica concentration (120 ppm) along with magnesium and targeting at high recovery. pH 7 and no antiscalants were used in all the feed solutions. It was theorized that those unfavorable conditions would push the system

to the limit, allowing that way the more comprehensive study of potential scaling occurrence and would enable the straightforward examination of CCRO tendency to resist and retard silica scaling. Supplementary to the filtration tests, batch experiments simulating various brine conditions were performed in order to test the effects of important factors such as the pH and hardness ions. The main research question of the current study can be formulated as follows.

What is the efficiency of CCRO in withstanding and delaying silica scaling during treatment of silica supersaturated waters?

In order to answer the main research question, the following sub-questions can be formulated.

- What is the effect of pH on scaling potential?
- What is the effect of hardness ions on scaling potential?
- What is the effect of silica supersaturation level on scaling potential?
- How does the form of silica influence the scaling potential?
- What is the performance of CCRO as compared with conventional RO in terms of silica scaling retardation?

2

Theoretical background

2.1. Closed-circuit reverse osmosis (CCRO)

Closed-circuit reverse osmosis (CCRO) or closed-circuit desalination (CCD) is based on the same basic principles as the conventional reverse osmosis (RO) technology, yet applying a different configuration. Figure 2.1 [16] depicts the typical configuration of a CCRO system. Feed water becomes pressurized by means of a high pressure pump and passes through the membrane elements, where it splits into a purified permeate and a concentrate stream. The latter is recirculated via a recirculation pump and mixed with the fresh feed before entering the pressure vessel again. Concentrate recirculation lasts until the required recovery has been reached, at which point the brine discharge takes place through the three-way valve opening. CCRO operating parameters can effectively be controlled by the system's main constituents. More specifically, flux can be adequately regulated via the high pressure pump, whereas the cross-flow velocity via the recirculation pump. Finally, proper opening or closing of the brine valve allows for the desired recovery to be achieved. CCRO is commonly reported as a semi-batch RO process, owing to the continuous introduction of fresh feed water replacing the water that exits the system as permeate [10].

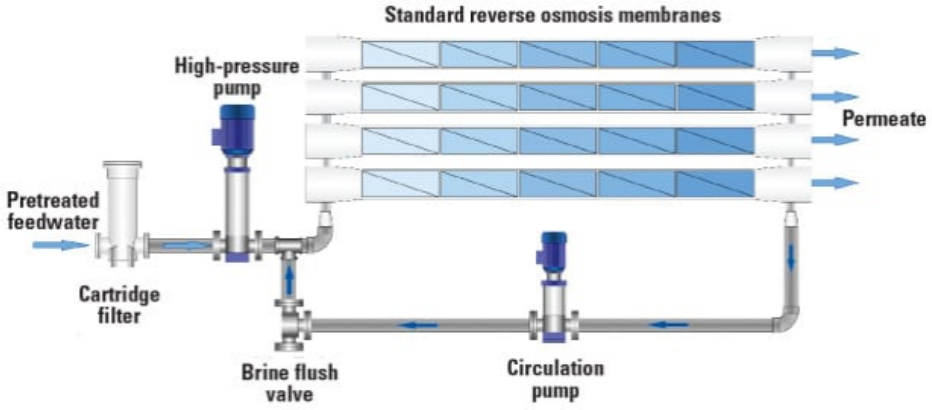

Figure 2.1: Representation of a typical CCRO system [16].

During a CCRO operation two modes alternate, viz. the closed-circuit desalination (CCD sequence) mode and the plug flow desalination (PFD sequence) mode. Most of the time, the system operates in CCD mode, during which the brine valve remains closed forcing the concentrate to be recirculated inside the system, while at the same time permeate is produced with an equal flow rate as the freshly introduced feed solution. After a predefined set point has been reached, denoting a specific recovery grade, CCD mode shifts to PFD mode. Several parameters could be employed as triggers for the PFD activation, such as the generated permeate volume, the electrical conductivity of the concentrate or the permeate, the applied pressure or even a pre-selected sequence duration [13]. When PFD

initiates, the recirculation pump stops while the three-way valve opens allowing for the concentrate disposal. At the same time, fresh feed compensates for the brine leaving the system. Despite the fact that during PFD some permeate is also produced, this specific mode is chiefly dedicated to the system rinsing. A schematic representation of the succession between the aforementioned operation modes is demonstrated in Figure 2.2 [17].

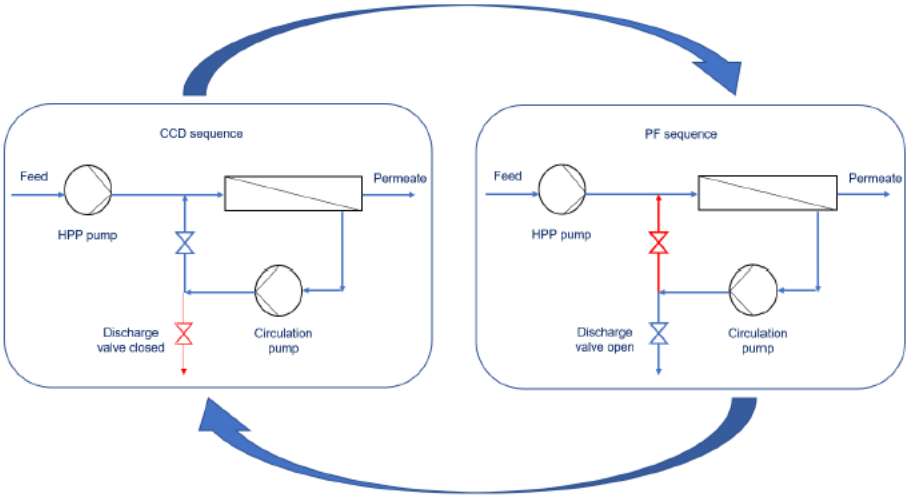

Figure 2.2: Alternation between the CCD/PFD modes [17].

The desalination process by means of the CCRO configuration is conducted in consecutive batches, often termed as sequences in the relevant literature. As previously mentioned, about 90% of the total sequence time is occupied by the CCD mode, which corresponds to the main desalination process, since PFD primarily serves for flushing. During that period, water is recycled inside the system and each complete circulation is referred to as cycle. Thus, a single CCD sequence consists of several cycles [18]. As sequence time passes, recovery increases, while the concentrate salinity rises and permeate quality deteriorates. Correspondingly, the applied pressure displays a gradual rise following the osmotic pressure growth path, in cases that constant flux is required, otherwise flux steadily drops, in cases that a constant applied pressure is maintained. The PFD flushing period lasts for roughly 10% of the total sequence time, during which the feed flow is higher than the feed flow during CCD to compensate for the loss of the circulation stream and to increase the cross flow over the membranes. Normally, one up to two system volumes are used for the system flushing.

In order to describe the system performance during the CCD mode, the following relationships can be applied [8]. Initially, a single cycle duration (t_{cycle}) is given by Equation (2.1). As follows from it, t_{cycle} remains fixed throughout the whole process.

$$t_{cycle} = \frac{V_{sys}}{Q_{recirc}} \tag{2.1}$$

,where V_{sys} corresponds to the intrinsic volume of the system (consisted of the pressure vessels and pipes capacity), whereas Q_{recirc} represents the recirculation flow rate regulated by the recirculation pump.

The duration of an entire batch sequence (t_{seq}) can then be estimated by the duration of a single cycle times the number of cycles constituting the batch sequence, as shown in Equation (2.2).

$$t_{seq} = N\frac{V_{sys}}{Q_{recirc}} \tag{2.2}$$

,where N represents the total number of cycles comprising a single batch sequence.

Further, the permeate volume produced per given sequence (V_p) is provided by Equation (2.3).

$$V_p = Q_p t_{seq} \tag{2.3}$$

,where Q_p stands for the permeate flow rate.

As mentioned above, during CCD the permeate flow rate equals the fresh feed flow rate entering the system, marked as $Q_{f,fresh}$ in Equation (2.4). Hence, the recovery accomplished during a CCD sequence (R_{seq}) can be calculated via Equation (2.5).

$$Q_{f,fresh} = Q_p \tag{2.4}$$

$$R_{seq} = \frac{V_p}{V_{f,fresh} + V_{sys}} = \frac{V_p}{V_p + V_{sys}} \tag{2.5}$$

Regarding the module recovery (MR), it can be estimated from Equation (2.6).

$$MR = \frac{Q_p}{Q_{f,fresh} + Q_{recirc}} = \frac{Q_p}{Q_p + Q_{recirc}} \tag{2.6}$$

Eventually, by combining Equations (2.3) and (2.5), a relation between sequence duration and recovery can be formulated as follows.

$$t_{seq} = \frac{R_{seq} V_{sys}}{Q_p (1 - R_{seq})} \tag{2.7}$$

As far as the system operation during the PFD mode is concerned, a usual mass balance can be applied, since during that period CCRO operates as conventional RO, as shown in Equation (2.8).

$$Q_{f,fresh} = Q_p + Q_c \tag{2.8}$$

,where Q_c stands for the concentrate stream, which during the PFD mode is discharged and not recycled back in the module inlet.

Finally, Equation (2.5) refers to the recovery achieved during a CCD sequence. In order to calculate the total system recovery both the PFD and CCD sequences should be considered, as shown in Equation (2.9).

$$R_{sys} = \frac{V_{pPFD} + V_{pCCD}}{V_{f,fresh}} \tag{2.9}$$

,where V_{pPFD}, V_{pCCD} the permeate volumes produced and $V_{f,fresh}$ the total feed volume consumed during both sequences. Since during PFD most of the feed water is wasted, prolonged flushing periods lead to lower total system recoveries. Therefore, typically the minimum flushing time corresponding to one system volume is applied.

2.1.1. CCRO in comparison to conventional RO

In this part, CCRO is contrasted with conventional RO principally in the light of the process itself, the corresponding costs, the operation flexibility as well as the fouling and scaling potential associated with the two configurations.

As far as the process characteristics are concerned, conventional RO comprises a continuous process which operates under steady state conditions, thus the quality of both the concentrate and the permeate streams remain unchanged throughout the process. On the other hand, the semi-batch CCRO operates under time-varying conditions due to the brine recirculation, resulting in a gradual increase of the salinity in both the concentrate as well as in the permeate side, as the sequence progresses. Subsequently, recovery in CCRO is a function of the elapsed operation time or in other words of the number of the performed cycles. In contrast to that, the recovery achieved in a conventional RO system depends on the number of stages or the number of membrane elements placed in series. All in all, CCRO requires just a single stage to reach virtually any desired recovery grade, which allows for better flux distribution contrary to multistage RO operations [18].

Additionally, the need for merely one stage in CCRO systems enables the avoidance of extra costs associated with supplementary stages' equipment, such as pressure vessels, membranes and various gauges. Moreover, in conventional RO a lot of energy is wasted through the concentrate disposal. This amount of energy is restored in the case of CCRO, where the brine is recycled and mixed with the incoming fresh feed. This manifests a twofold advantage, since it eliminates the need for ERD on the one hand as well as significantly reduces the amount of feed water in need of being pressurized by the high pressure pump on the other. Both of them are translated into important cost and energy savings [11]. Besides, the gradual salinity rise enables the concurrent gradual applied pressure increase, following the osmotic pressure gradients, reaching its maximum value only at the end of each sequence. Contrary to that, conventional RO works at the highest required pressure throughout the entire operation. Overall, according to what many studies have reported, CCRO exploits the available energy in a more efficient way and therefore it is accompanied by lower cost burden as compared to conventional RO [9].

Another substantial asset of CCRO comprises its great flexibility regarding the control of the system operational parameters. Particularly, via the system's main constituents, the cross-flow velocity as well as the recovery can be readily adjusted without affecting the flux. This makes CCRO systems considerably versatile and renders them less sensitive to feed water variations as compared to conventional RO, in which recovery, flux and cross-flow velocity are coupled and therefore especially difficult to be adjusted individually [12].

The preceding discussion partly revealed the reasons why CCRO has been considered to be highly fouling and scaling resistant. Initially, the high cross-flow velocity owing to the concentrate recirculation creates turbulence which disturbs the stagnant layer close to the membrane surface, reducing in that way the concentration polarization layer [12]. It has been also theorized, that the regular system flushing at the end of each sequence delays or even prevents scaling, since there is no sufficient time for salts to precipitate out of the supersaturated solution. Lastly, it has been suggested that the large salinity variations inside the loop create unfavorable conditions for microorganisms to develop and grow, hampering that way biofouling [12].

2.2. Silica aqueous chemistry

An essential reason behind the difficulties that many desalination facilities face to address silica scaling issues, certainly stems from the complexity of the chemistry governing silica polymerization as well as scale formation. Thus, a deeper understanding of the underlying mechanisms comprises the foundation upon which improved innovative techniques aiming at silica scale mitigation could be developed. To that end, the following section seeks to shed light on the complex issue of silica aqueous chemistry.

2.2.1. Silica in natural waters and silica speciation

Silica comprises a natural constituent often encountered in many water resources, worldwide. This fact comes as direct consequence of the abundance of silicon (Si) in the Earth's crust (being the second most abundant element after oxygen). However, Si rarely occurs as pure element and therefore it can be usually found in numerous other forms, such as silica (SiO_2) and various silicates. Under the term silica, a wide range of different species with distinct characteristics are included. For instance, in terms of the molecular structure crystalline silica and amorphous silica can be distinguished, whereas in terms of size monomeric, polymeric, colloidal and particulate silica can be encountered [19].

The form in which silica occurs in water comprises a crucial parameter as far as its precipitation potential is concerned. Initially, amorphous silica is mainly of interest for RO applications, since crystalline silica, such as quartz, displays a particularly low solubility in water, in the order of 5 - 6 mg/L [20]. Naturally, amorphous silica ends up in groundwater after dissolution of silicate minerals in the subsoil through a hydrolysis reaction. A depiction of the reversible dissolution hydrolysis reaction is provided in Figure 2.3 [21]. Although the dissolved quantity may contain multiple forms at near neutral pH values and ambient temperatures, it primarily consists of monomeric silica, also termed as monosilicic or silicic acid, reactive and soluble silica. Hence, the dissolved silica in solution can be principally described by the chemical formula $Si(OH)_4$ or H_4SiO_4. The silanol groups (-Si-OH) of monosilicic acid are responsible for the reactivity that this compound exhibits [19]. Under supersaturated conditions, reactive silica undergoes a polymerization process, during which individual silicic acid molecules bind to each other via a dehydration reaction forming dimers, trimers and other low molecular weight oligomers. This

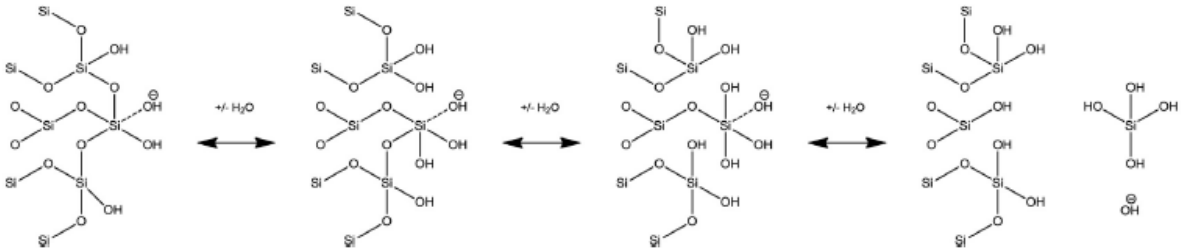

Figure 2.3: Silica reversible dissolution mechanism [21].

form of silica is then referred to as polysilicic or polymeric silica and it is considered to be particularly unstable in solution [19]. If silica polymers continue to grow, through initially linear and subsequently circular structures, tiny spherical particles are generated, namely colloidal silica. According to IUPAC classification, particles with diameters between 0.001 and 1 μm are characterized as colloids. Those colloids are non-reactive and especially stable in solution due to their negative surface charge, in a wide range of pH values. Under certain conditions, colloids can agglomerate or further crystallization on their surface may occur leading to the creation of larger particles, categorized as particulate silica. In practice, particulate silica can be separated from the solution by means of a 0.45 μm filter [22]. An overview of the various silica forms, along with some characteristics of theirs, is presented in Table 2.1.

Table 2.1: Overview of the various silica forms encountered in aqueous solutions.

Silica form	Size	Characteristic
Monomeric	Consists of a single H_4SiO_4 unit.	Main form of dissolved silica in natural waters in concentrations below 200 mg/L.
Polymeric	Consists of two or more than two and often up to four monomeric units.	It has a transient presence in solution, since it is particularly unstable.
Colloidal	Many units combined in circular structures forming spherical particles with diameters in the range of 0.001-1 μm.	Colloids are stable in solution due to their negative surface charge in a wide range of pH values.
Particulate	Large polymers formed after colloids aggregation.	They can be separated from the solution by means of a 0.45 μm filter.

2.2.2. Factors affecting silica speciation and solubility

Silica solubility is directly related to the form that it is present in water. Solubility of amorphous silica has been reported to be in the range of 100 to 140 ppm, at 25^{o}C [23]. Nonetheless, the actual solubility depends on several parameters. The most important factors controlling silica speciation and thus directly affecting its solubility are the temperature, the pH, the presence of multivalent metal ions, the solution's ionic strength as well as the silica concentration itself.

As aforementioned, silica found in natural waters occurs primarily in its monomeric form. Since monosilicic acid constitutes a weak acid (pK = 9.83, at 25^{o}C), at neutral and acidic pHs the predominant species is non-ionic. However, at higher pH values rapid deprotonation begins to take place, converting non-ionic species into ionic one. This transformation can explain the increased silica solubility (owing to electrostatic repulsions) observed at higher pH values, as illustrated in Figure 2.4 [21]. In addition to the effect of pH on solubility, pH influences the polymerization rate as well. Specifically, higher pH values facilitate silica polymerization, since hydroxyl ions promote the deprotonation reaction. This is of importance, since it has been theorized that reactions involving non-ionic with ionic monomers are favored over those between two non-ionic ones [21]. Thus, the precipitation potential increases via the shortening of the induction time related to the nucleation reaction. However, when pH increases

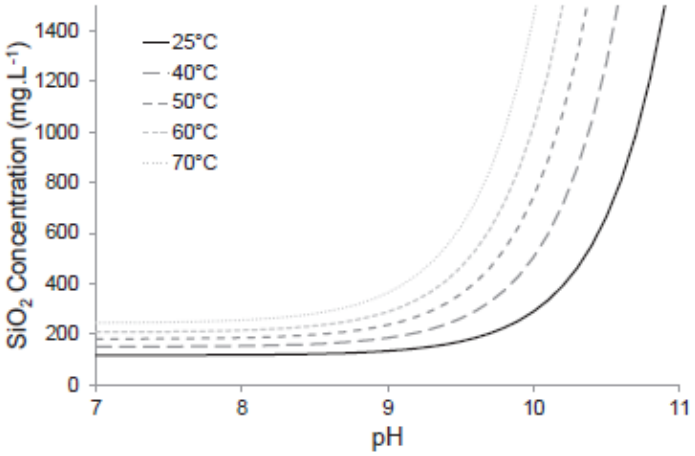

Figure 2.4: Amorphous silica solubility dependence on pH and temperature assuming no other salts are present in solution [21].

further most of the monomers become ionized and polymerization rate diminishes again. On the other hand, at low pH values extended induction times have been observed, due to the slower interactions between unionized monomers [24].

As far as the effect of temperature is concerned, silica solubility increases with increasing temperature. The results presented in Figure 2.4 manifest the temperature influence on silica solubility. Nevertheless, similarly to the pH effect, higher temperatures also stimulate a more rapid polymerization rate, which apparently counteracts the increased solubility effect in terms of scale formation potential [23].

Other constituents often present in natural waters can also significantly impact silica solubility, due to their interactions with silica. Hardness appears to have a twofold effect on scaling potential, by both decreasing silica solubility as well as increasing the polymerization rate. The formation of magnesium and calcium silicates owing to electrostatic attractions and/or adsorption of silica monomers onto magnesium and calcium hydroxides, at elevated pHs, can lead to declined solubility levels. The formation reactions of some common metal silicates are demonstrated in Figure 2.5 [25]. What is more, the stability of colloidal particles at a wide range of the pH spectrum (owing to their surface negative charge) can be disrupted by the presence of metal cations, such as Na^{+}, Mg^{2+} and Al^{3+}, which effectively neutralize the surface charge facilitating that way the aggregation between the colloids and subsequently the formation of larger polymers and particulates [26]. This process proceeds via the suppression of the so called diffuse double layer in the surface of the colloids. Finally, beyond the particular cations effect described above, an overall increase of the solution's ionic strength would also contribute to reduced silica solubility owing to the salting out effect [27].

$$\mathrm{Si(OH)_4 + Si(OH)_4 \rightarrow {}_3(HO)\text{-}Si\text{-}O\text{-}Si\text{-}(OH)_3 \rightarrow Oligomers \rightarrow (SiO_2)_n\ (silica\ polymer)}$$
$$\mathrm{+\ Al(OH)_3 \rightarrow {}_3(HO)\text{-}Si\text{-}O\text{-}Al\ (OH)_2 \rightarrow {}_3(HO)\text{-}Si\text{-}Al(OH)\text{-}O\text{-}Si(OH)_3 \rightarrow \rightarrow\ (Al\ silicate)}$$
$$\mathrm{+\ Fe(OH)_3 \rightarrow {}_3(HO)\text{-}Si\text{-}O\text{-}Fe(OH)_2 \rightarrow {}_3(HO)\text{-}Si\text{-}O\text{-}Fe(OH)\text{-}O\text{-}Si\text{-}(OH)_3 \rightarrow \rightarrow\ (Fe\ silicate)}$$
$$\mathrm{+\ Mg(OH)_2 \rightarrow {}_3(HO)\text{-}Si\text{-}O\text{-}Mg\text{-}OH \rightarrow {}_3(HO)\text{-}Si\text{-}O\text{-}Mg\text{-}O\text{-}Si(OH)_3 \rightarrow \rightarrow\ (Mg\ silicate)}$$
$$\mathrm{+\ Ca(OH)_2 \rightarrow {}_3(HO)\text{-}Si\text{-}O\text{-}Ca\text{-}OH \rightarrow {}_3(HO)\text{-}Si\text{-}O\text{-}Ca\text{-}O\text{-}Si(OH)_3 \rightarrow \rightarrow\ (Ca\ silicate)}$$

Figure 2.5: Formation reactions leading to silica and common metal silicates [25].

Finally, it has been reported that higher silica concentrations have been linked to faster polymerization rate, because a larger number of monomeric molecules is available for participating in the polymerization reactions. However, the generally slow speed that polymerization takes place, especially at ambient temperature, gives often rise to stable supersaturated solutions displaying concentrations well above the theoretical solubility limit [28]. In Table 2.2, the previously reported factors are encapsulated, which drastically influence silica solubility in aqueous solutions.

Table 2.2: Overview of the main factors affecting silica solubility.

Factor	Effect on solubility
pH	• At higher pHs: Increased solubility but also increased polymerization rate up to ∼pH 9 when it starts dropping again. • At lower pHs: Decreased solubility but also decreased polymerization rate.
Temperature	Increased solubility but also increased polymerization rate.
Hardness	Reduced solubility due to metal silicates formation. Additionally, hardness promotes colloids agglomeration.
Ionic strength	Higher ionic strength leads to reduced solubility due to salting out effects.
Silica concentration	Higher initial silica concentration leads to higher polymerization rate.

2.2.3. Silica scaling in RO systems

Silica present in feed water can cause serious problems during RO applications when it deposits on the membrane surface inducing scaling. The deposition mechanisms as well as the created scale forms strongly depend on the specific type of amorphous silica contained in the solution. In cases of relatively low silica concentrations, the predominant species comprises monosilicic acid, as explained in Section 2.2.1. Although this monomeric form is for the most part stable up to concentrations of about 200 mg/L, it can potentially react with any available functional hydroxyl (-OH) group of the membrane surface, stick to it and serve as seed for crystallization. Subsequently, other monomers can adhere to this initial seed, effectively promoting polymerization on the membrane surface. The outcome of such a process comprises the creation of an impermeable glass-like film, which normally causes a rapid permeate flux decline. This mechanism of monomers adherence to the membrane surface is termed as homogeneous nucleation. In addition to that, direct monomers deposition can be assisted by non-silica colloids or other pre-existing scale. In this case, deposition and crystallization onset proceed via the so called heterogeneous nucleation [20].

Despite the fact that silicic acid deposition constitutes a potential scaling mechanism, the consensus remains that the key fouling driver at highly concentrated conditions (thus when the solubility limit of dissolved silica has been by far exceeded) comprises the polymerization of monomers creating polymers of colloidal size [20]. The formed colloids can collide with the membrane surface and loosely adhere to it, resulting in the creation of a thin porous layer. It is noted, that the exact mechanism is not well understood yet. Subsequently, the bound colloids can further adsorb new monomeric molecules causing additional thickening of the layer. Eventually, the created scale receives a gel-like form, which can turn to be harder and opaque over time [21]. The coating generated through this mechanism appears to be more porous and causes a more gradual flux decline, as compared with the mononomeric scaling process. In summary, the main distinguish between the two deposition mechanisms concerns whether polymerization takes place on the membrane surface or in the bulk solution [23]. Moreover, in both cases the presence of multivalent cations, such as magnesium or aluminum, facilitates silica precipitation, particularly under alkaline conditions. Regarding soluble silica, the precipitation mechanism at pH above 8.5 proceeds via the formation of insoluble metal silicates, when silicate anions react with positive metal ions present in the solution (due to electrostatic attractions) [29]. In the case of colloidal polymers, precipitation is promoted by the presence of divalent and trivalent cations, because they neutralize the colloids surface charge, accelerating in that way their agglomeration and the subsequent amorphous scale formation [30].

Lastly, it is noted that the concurrent action of both aforementioned fouling mechanisms is also feasible, namely deposition consisted of both monomeric as well as colloidal molecules. The relevant process in this case entails an initial attachment of colloids to the membrane surface followed by monomers adsorption onto them. This type of scaling is considered to be particularly hard and adherent [21].

2.3. Scaling detection and mass transfer coefficient (MTC)

Scaling detection can practically be realized either through mass balance measurements of the sparingly soluble salts or via the normalized flux or mass transfer coefficient (MTC) monitoring. Since the first method comprises an expensive and laborious procedure, it is mostly applicable in pilot installations, whereas MTC monitoring has been common practice for full-scale facilities [31]. This method is essentially based on the inspection of the MTC variations over time and especially of the last membrane element (of the last stage in case of more than one stages) of a conventional RO system. This is because the last element experiences supersaturated conditions on a permanent basis between cleaning periods and therefore it is the most vulnerable to scaling. A typical time period between two consecutive cleanings is regarded one week or even longer [32]. When no scaling has taken place the MTC value remains constant, otherwise it faces a rapid or a more gradual decline, depending on the form and the extend of the fouling occurrence [33]. The calculation of the MTC is realized via Equation (2.10).

$$MTC = \frac{Q_p TCF}{A_{mem} NDP} \tag{2.10}$$

,where Q_p is the permeate flow rate, A_{mem} the membrane's active surface area, NDP the net driving pressure and TCF the temperature correction factor.The mass transfer coefficient is often expressed in (m/sPa) units, whereas in the relevant literature it can also be encountered as the membrane water permeability, K_w. The term (Q_p/A_{mem}) corresponds to the permeate flux, J_w, as shown in Equation (2.11).

$$J_w = \frac{Q_p}{A_{mem}} \tag{2.11}$$

The permeate flux, expressed as $(m^3/m^2 s)$ or most commonly as $(L/m^2 h)$, constitutes an important membrane performance parameter. Essentially, variations of the MTC represent alterations in the flux value, having first being normalized for the net applied pressure as well as corrected for potential temperature fluctuations. The net driving pressure is given by Equation (2.12).

$$NDP = TMP - \Delta_\pi \tag{2.12}$$

,where TMP stands for the trans-membrane pressure and Δ_π for the osmotic pressure difference across the membrane. Their calculation becomes possible via the following equations.

$$TMP = \frac{P_f + P_c}{2} - P_p \tag{2.13}$$

$$\Delta_\pi = \frac{\pi_f + \pi_c}{2} - \pi_p \tag{2.14}$$

,where P_f, P_c and P_p stand for the measured pressure values in the feed, concentrate and permeate side, respectively, while π_f, π_c and π_p refer to the osmotic pressure values in the corresponding membrane sides. As far as the temperature influence is concerned, it can be taken into account by means of the corrected flux at a selected reference temperature (e.g. at 20°C), which can be calculated by Equation [34].

$$J_{w,20^oC} = J_w e^{-0.0239(T-20)} \tag{2.15}$$

,where J_w is the actual measured flux and T the measured temperature.

As previously discussed, the occurrence of scaling in a system can be identified via the membrane permeability reduction and for that reason MTC is widely used as scaling indicator. In common industrial practice membrane permeability is estimated from Equation (2.10), however in reality it depends on various physical factors as can be seen in Equation (2.16) [35].

$$K_w = \frac{p d_{pore}^2}{8\tau l} \tag{2.16}$$

,where p is the membrane porosity, d_{pore} the pores' size, τ the tortuosity and l the membrane thickness.

Finally, besides scaling other phenomena could result in drop of the MTC value as well, such as non-scalant depositions or a potential osmotic pressure build-up on the membrane surface caused by the concentration polarization (CP) phenomenon, which can be described as the gradual accumulation of retained ions in a stagnant layer close to the membrane surface. This is because those effects add an extra resistance to the water flux and thus a higher feed pressure is required in order to overcome it. Nonetheless, the noticeable difference in those cases, as opposed to scaling occurrence, lies in the fact that the original MTC value can be easily restored.

3

Materials and methods

3.1. Batch experiments

In previous study conducted at TU Delft [15] investigating silica scaling in CCRO systems, highly concentrated silica solutions (ranging from 70 mg/L to 120 mg/L) were tested at high recovery operations. It was revealed that even at an initial silica concentration of 120 mg/L and up to a 93% recovery grade no scaling occurred. Aiming at more closely investigating the prevailing conditions in the concentrate of a CCRO system and relating them to the precipitation potential, a campaign of several batch tests was carried out. In those tests, not only the different silica supersaturations were considered, but also the effect of common brine constituents such as magnesium and calcium ions. The experimental process begun without pH adjustment of the prepared solutions so as to simulate the exact conditions of the aforementioned study [15], thus pH values above 10 prevailed in those cases, since sodium silicates produce alkaline solutions. Additionally, batch runs at near neutral pH (∼7) were conducted in order to simulate the brine conditions of the CCRO experiments performed in the current study.

As aforementioned, the objective of the batch tests was the simulation of the actual conditions prevailing in the final brine of each sequence. At that point, just before the brine discharge takes place, the highest salinity level during a CCD sequence can be encountered and therefore the risk of scaling is the greatest. Of course, due to the time-varying conditions this maximum salinity is practically experienced only for several minutes towards the end of each CCD sequence. However, in order to gain insight into the most adverse conditions (in terms of precipitation potential) all the prepared batch compositions corresponded to those of a final brine. According to the industrial guidelines, the maximum recommended duration of a CCD sequence is less than one hour (∼50 min). In this case, though, in order to study silica polymerization over a longer period of time, each experimental run was chosen to last 4 hours. During each run, a total of ten samples was collected in duplicates, six of which during the first hour in order to detect concentration variations occurring within the usual duration of a CCD sequence. Lastly, the precipitation potential was implicitly inferred by examining the extent of polymerization. In its turn, this was monitored by regularly measuring the concentration of monomeric silica throughout the experimental duration, by means of the silicomolybdate method.

Various solutions were prepared, simulating brines theoretically emerging from two different solutions with nominal initial concentrations 70 mg/L and 120 mg/L SiO_2, respectively, after three distinct recoveries had been achieved, viz. 80%, 85% and 90%. In some of the batches hardness cations were added as well, either separately or collectively to each other. In cases where Mg^{2+} and/or Ca^{2+} were present, their concentration corresponded to a nominal initial quantity of 1 mM each, equivalent to 24 mg/L and 40 mg/L, respectively. The realized batch experiments are summarized in Table 3.1, indicated by the symbol x. For instance, the simulation of a brine emerging from a solution initially containing 70 mg/L SiO_2 and 24 mg/L Mg^{2+} at 90% recovery (CF=10), corresponded to a prepared concentration in the batch of roughly 700 mg/L SiO_2 and 243 mg/L Mg^{2+}. In practice, the average values of the calculated theoretical concentrations and of projected values provided by the LewaPLus software were used. In Table 3.1, with single x are marked the batches which were conducted without pH adjustment (thus at pH>10), whereas with double x those performed at both high pH as well as at pH 7. In Table A.1 of Appendix A, the exact concentration values of SiO_2, Mg^{2+} and Ca^{2+} used in the

performed batch tests are demonstrated.

Table 3.1: Overview of the conducted batch tests. Single x indicates batches performed without pH adjustment, whereas double x batches performed both with and without pH adjustment. The initial concentration of each of Mg^{2+} and Ca^{2+} was 1 mM.

Theoretical initial concentration	80% R	85% R	90% R
SiO_2 (70 mg/L)	x	x	-
+ *Mg*	xx	xx	-
+ *Ca*	x	xx	-
+ *Ca/Mg*	x	x	-
SiO_2 (120 mg/L)	x	x	x
+ *Mg*	xx	-	-
+ *Ca*	x	-	-
+ *Ca/Mg*	-	-	-

The experimental runs proceeded as follows. The batch tests took place in 500 mL covered plastic beakers, so as to avoid potential solution contamination in case that glassware was used. For each run, the required amount of sodium metasilicate was dissolved in demineralized water and when the effect of Ca^{2+} and/or Mg^{2+} was also studied, calcium chloride and magnesium chloride salts were dissolved in demi water in a separate beaker and then added into the silica solution. Moreover, whenever pH adjustment was necessary, it was realized in the initial silica solution prior to the addition of the hardness ions. Afterwards, the prepared solution was placed on a magnetic stirrer and continuously mixed at a rotational speed of 150 rpm. All the experimental runs were carried out at room temperature, which was in the range of 17 – 20.5^{o}C. Throughout the 4 hours of each test, samples were periodically collected in duplicates, using plastic syringes (BD) bearing 0.20 μm filters (VWR) on them, in order to remove the created insoluble particles. The first few ml of every sample were discarded so as to prevent any potentially trapped silica in the filter from ending up in the sample. Next, a sufficient portion of each filtered sample was transferred into a clean plastic container by means of a pipette (Thermo Electron) and adequately diluted with demi water until a total volume of 10 ml. Dilution was essential for the following specimen measuring according to the silicomolybdate method. Whenever the reactive silica measurement was impossible shortly after the experiment completion, samples were stored in the refrigerator for their later analysis. Based on the silicomolybdate method results, graphs of the soluble silica concentration variations over the 4 hours of each experimental run were produced. Additionally, targeting at obtaining insight into the impact of hardness ions on the polymerization process, their concentration changes were also monitored during some designated tests, by analyzing the periodically collected samples with ion chromatography (IC).

3.2. CCRO experimental process

3.2.1. Description of the CCRO setup

The front and back view of the setup used to perform the CCRO tests, provided by Lenntech B.V., are shown in Figure 3.1, in which its main components are illustrated as well. A simplified schematic overview of the setup is shown in Figure 3.2, while a summary of its parts is presented in Table 3.2. During a CCD operation, the synthetic feed water was initially pushed by the feed pump through the 5 μm cartridge filter (Suez Purtrex) before its further compression by means of the high pressure pump (HPP) forcing it to pass through the single-module RO membrane. It is pointed out, that cartridge filters constitute an integral part of RO systems, serving to protect the high pressure pumps as well as the membranes from potential impurities present in the feed water. The produced permeate was discharged directly to the sewer, whereas the concentrate was recycled back and blended with the fresh feed by means of the recirculation pump, which compensated for the pressure losses inside the pressure vessel (PV). At the end of each sequence the automatic brine valve opened, allowing for the brine disposal into the sewer. The feed pump comprised a Grundfos centrifugal booster pump

adjusted to provide a constant pressure of 2 bar. Both the high pressure and the recirculation pumps were controlled via two variable frequency drives (VFD), located inside the control cabinet. Concerning the former, it was a Fluid-o-Tech stainless steel rotary vane pump, capable of delivering flow rates in the range of 100 – 260 L/h and up to 20 bar of head. Regarding the latter, it was a Grundfos centrifugal pump exhibiting a maximum flow rate capacity of about 1650 L/h and a pressure head of 20 bar. The highest admissible operating pressure that the entire system could withstand was 16 bar.

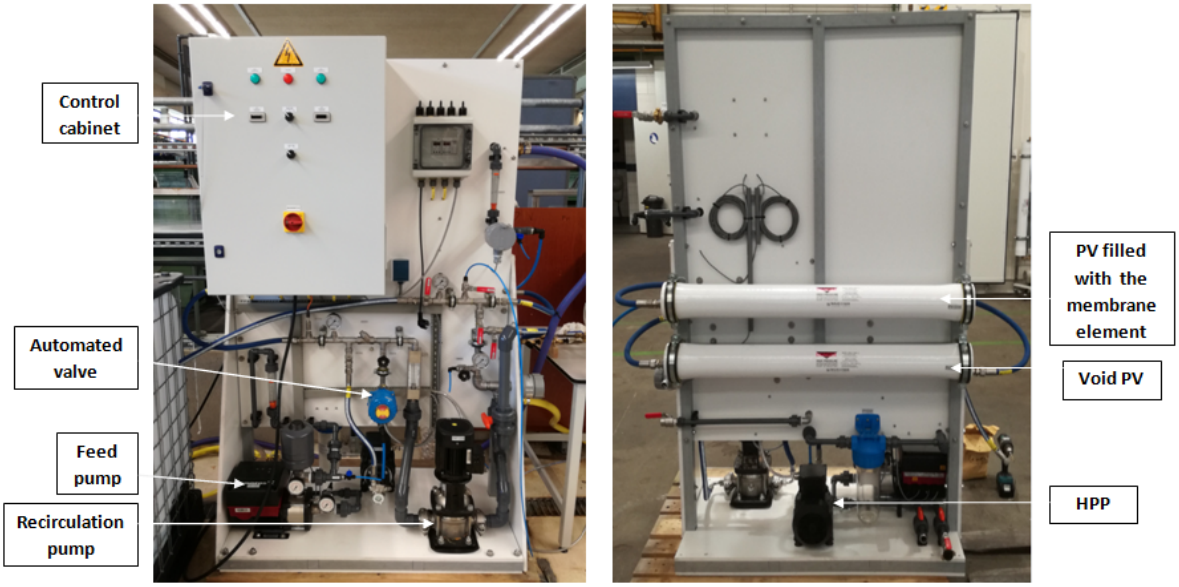

Figure 3.1: Front and back view of the experimental setup provided by Lenntech B.V.

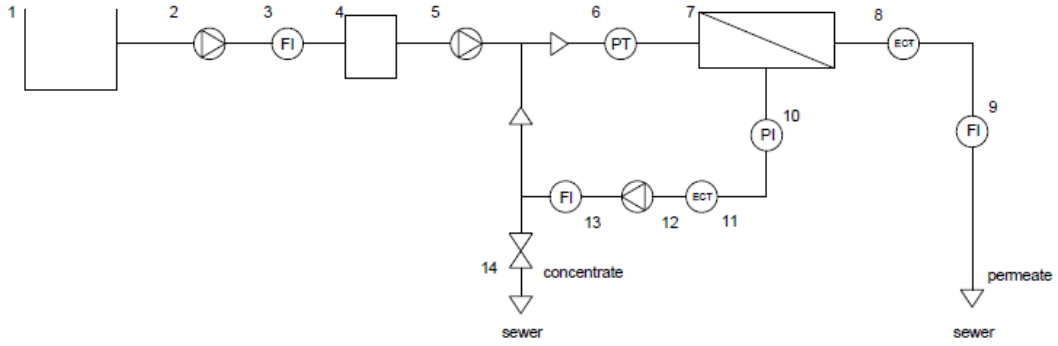

Figure 3.2: Schematic overview of the CCRO experimental setup.

As shown in Figure 3.1, two pressure vessels (Wave Cyber) were mounted on the experimental skid, yet only the top one was filled with the membrane element, whereas the bottom one was kept void. This layout constitutes common practice for industrial CCRO facilities in order to keep an empty space (spacer) inside the pressure vessel, in a position where a membrane element should theoretically exist, increasing that way the intrinsic volume of the system. This is of importance especially for low recovery operations, so as to comply with recommended system operating parameters (e.g. admissible flow rate limits provided by projection softwares). In the case of the current setup, an additional PV was added to achieve the system's intrinsic volume expansion, because only a single membrane could fit inside each pressure vessel. For the present study the additional empty space was not required and the isolation of the void PV from the rest of the process line was made possible by means of proper connections and valves. Lastly, the FILMTEC^{TM} BW30-4040 element of the Dow company was used throughout the experimental process. The main membrane features are provided in Table 3.3, whereas the specification data sheet is available in Appendix B.

Table 3.2: Description of the CCRO setup parts.

Number	Abbreviation	Description
1		Feed tank
2		Feed centrifugal pump
3	FI	Flow indicator of the fresh feed
4		Cartridge filter with mesh size 5 μm
5		Positive displacement high pressure pump
6	PT	Pressure transmitter in the combined stream
7		Membrane module
8	ECT	Electrical conductivity transmitter in the permeate stream
9	FI	Flow indicator in the permeate stream
10	PI	Pressure indicator in the concentrate stream
11	ECT	Electrical conductivity transmitter in the concentrate stream
12		Recirculation centrifugal pump
13	FI	Flow indicator in the concentrate stream
14		Automatic brine valve

Table 3.3: Membrane main features.

Product name	BW30-4040
Type	Polyamide thin-film composite
Length	1016 mm
Active area	7.2 m^2
Salt rejection	99.5 %
Surface charge	Negative
Maximum operating pressure	41 bar
Maximum feed flow rate	3.6 m^3/h
pH operating range	2 - 11

As far as the required measurements are concerned, the flow rates were monitored through three flow meters (Stubbe, Kytola) located in the fresh feed, permeate and concentrate side, respectively. Hence, the mixed feed flow (after the two steams blending) could be calculated by adding the fresh feed and the recirculated brine flow rates. The pressure drop taking place inside the pressure vessel was monitored by means of two pressure gauges (WIKA) with measuring range 0 – 10 bar, situated in the inlet and the outlet of the PV. Regarding the permeate, it was leaving the system uncompressed, at atmospheric pressure. What is more, two inline digital conductivity sensors (ASTI) placed in the concentrate and the permeate sides provided continuous readings of the respective electrical conductivity (EC) and temperature values, displayed on the panel screen also mounted on the setup skid. The required EC, temperature and pH values of the feed solution were measured prior to the beginning of each experimental run, by collecting a sample straight from the IBC feed container and immediately analyzing it. Based on the acquired fresh feed and concentrate EC values, the EC of the mixed feed could be calculated as well, by applying a salt mass balance.

3.2.2. Experimental procedure

The tank used to store the prepared solutions was a 1000 L IBC container. In order to ensure a proper mixing of the final solution for each experimental run, it was prepared in batches employing a smaller container of 60 L. In this smaller container the appropriate weighed amount of sodium silicate was dissolved in pure water up to the desired concentration. The dissolution of sodium silicate induced a steep rise of the solution pH, which received values between 11 and 12. In order to avoid the instant formation of magnesium hydroxide flocs, the pH adjustment (using HCl acid) preceded the $MgCl_2$ addition. Particularly, pH was first lowered to a neutral level (close to 7). After the pH adjustment, $MgCl_2$ powder was first dissolved in demineralized water inside a different plastic beaker and then poured into the initial sodium silicate solution. The separate preparation of the two solutions was intended to enhance the mixing efficiency. Finally, after additional stirring of the 60 L container by the operator, the prepared mixture was poured into the IBC tank. The whole process was repeated several times until the feed tank was filled with the required solution volume. Aiming at the highest homogeneity of the final solution as possible, the prepared mixture was kept in the IBC container for as long as one day prior to the beginning of each experimental run.

The operational protocol followed to perform the CCRO experiments was as follows. At the beginning of each filtration test, the feed pump was activated and was left to operate for about one minute (time needed to stabilize at 2 bar of constant provided pressure), after which the toggle switch, located on the control cabinet front, was turned by the operator into the PFD mode. This first PFD sequence, also termed as Power-Up Rinse (PUR), targeted at flushing out the system from remaining water since the last setup usage. It is emphasized that the entire system was time-based operated. Thus, when the PUR started, the respective PFD timer was activated as well. During that period, the circulation pump was off, while the high pressure pump (HPP) operated according to the PFD set point. This had been previously adjusted by means of the respective VFD, in order to provide a steady feed flow rate of 180 L/h. The permeate flow rate during the PFD mode could be regulated via the manual valve and was set to about 30 L/h, translating into a $\sim$17% recovery grade. The duration of PFD was selected to be 4 min, a sufficient time for the entire system volume to be replaced by fresh feed and thus for an effective system rinse to be accomplished. The intrinsic volume of the system (V_{sys}) was estimated to be about 8 L, which means that the chosen flushing time corresponded to 1.5 system volumes. Once the predetermined PFD time had passed, the toggle switch was manually turned into the CCD mode, followed by the CCD timer activation. The operation time of CCD was directly related to the desired recovery grade and its choice was essentially based on preliminary filtration tests, as will be later explained (see Section 3.3.2). During the CCD process, the delivered by the HPP fresh feed flow ($Q_{f,fresh}$) dropped to 110 L/h, whereas the permeate flow (Q_p) was roughly identical to that, signifying a theoretical recovery grade of 100%. Moreover, the recirculation flow rate (Q_{recirc}) was constantly maintained at 1200 L/h. Based on those flow rate values, the permeate flux as well as the module recovery during CCD could be defined, which were $\sim$15 L/m^{2}h (or lmh) and $\sim$8.4%, respectively. After the selected time had passed, the toggle switch was turned once again into the PFD mode, allowing for the system rinsing prior to the beginning of the following CCD sequence. This alternation between the two system operational modes was carried on for as many sequences as required for the specific experimental series to be completed. After the final CCD run, a PFD sequence was always performed, often termed as the Shutdown Flush (SDF). This closing flush was absolutely necessary in order to ensure that no highly saline concentrate would remain inside the module for as long as the system would stay in shutdown mode, increasing in that way the risk for scaling. Besides, aiming at a more efficient final cleaning, SDF was carried out using demi water for about 10 min, instead of the feed solution which was generally employed during the PFD rinsing.

In Section 3.2.1 the CCRO setup's measuring instruments were described. Through them, the required values monitoring and recording took place periodically throughout each CCD sequence. The recorded values comprised the feed pressure of the mixed stream in the module inlet ($P_{f,mixed}$), the permeate electrical conductivity (E_{C_p}) and temperature (T_p) as well as the concentrate pressure (P_c), electrical conductivity (E_{C_c}) and temperature (T_c). What is more, due to some discrepancies observed of the fresh feed and permeate flow rates from the respective set values, $Q_{f,fresh}$ and Q_p were regularly recorded as well. The collected data were then kept for their further analysis. During the PFD operation no measurements were performed. Finally, at the end of each sequence a sample from the final brine was taken so as to be analysed for its monomeric silica content, by means of the silicomolybdate method. The sample was collected from the loop, at the time just before the valve was opened allowing

for the brine discharge. In Figure 3.3, the operation protocol of the overall experimental process is schematically summarized.

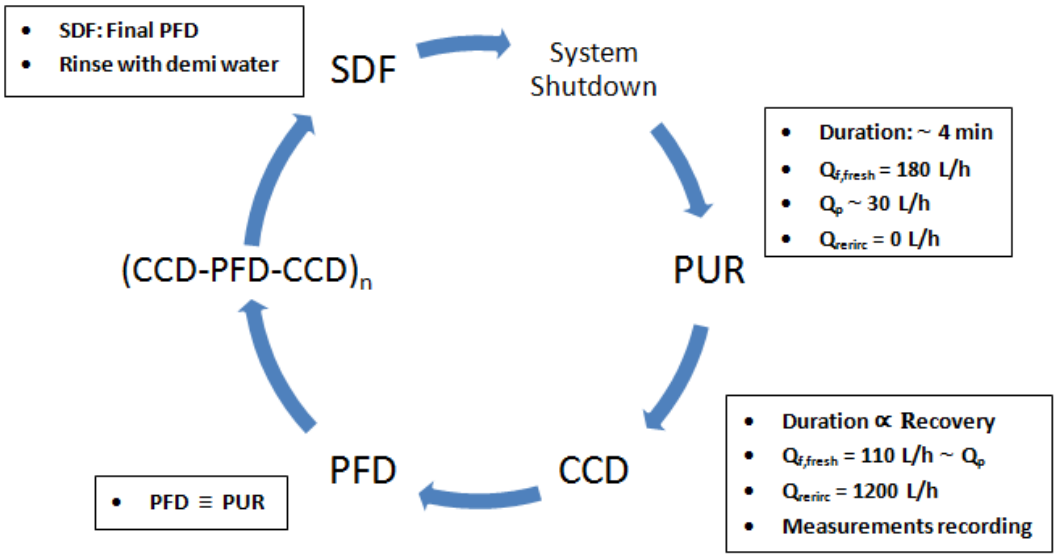

Figure 3.3: Operational protocol of the entire experimental process.

3.3. Conducted CCRO experiments

The main focus of the present study was the investigation of the CCRO systems potential to withstand scaling. This was realized by means of CCRO filtration experiments, which succeeded the conducted batch tests. Prior to the central part of the scaling tests themselves, the determination of both the clean membrane permeability as well as of the correlation between sequence time and recovery preceded.

3.3.1. Pristine membrane water permeability

The first set of experiments conducted employing the CCRO setup regarded the permeability determination of the pristine membrane. To this purpose, filtration experiments were performed at varying trans-membrane pressures (TMPs), using demineralized water as feed. Hence, osmotic pressure was considered equal to zero. Each TMP resulted in a different permeate flow and in that way the plot of the applied TMPs as a function of the derived fluxes was constructed. The slight temperature variations were taken into account by correcting the fluxes through Equation (2.15). The ratio of the permeate flux to the TMP provides the clean membrane water permeability or MTC, as was demonstrated by Equation (2.10). The membrane permeability test was carried out in the PFD mode, in which the various TMP values were regulated by means of the manual concentrate valve.

3.3.2. Concentration factor and recovery determination

In the theoretical part of this work, it was explained that recovery (R) and concentration factor (CF) in CCRO configuration are functions of time. The mathematical relation between CF and recovery is shown in Equation (3.1). It is therefore essential to determine the CCD sequence duration required for a specific CF to be reached. Prior to the experimental process, a first estimation had been provided by the LewaPlus projection software of the Lanxess company, which was employed for the preliminary system design. In order to verify the actual CF-time correlation, filtration experiments using solutions of magnesium sulfate ($MgSO_4$) dissolved in demi water were carried out. The whole process was based on the monitoring of the $MgSO_4$ concentration changes over time. Hence, the usage of magnesium sulfate as reagent was justified by the 100% rejection of the divalent Mg^{2+} and SO_4^{2-} ions by the BW30-4040 element. Two individual tests took place, during which samples were collected periodically from the recirculated concentrate and subsequently analyzed by means of the ion-exchange chromatography (IC). The acquired concentrations were then plotted against the respective sampling points in time and in that way the graph of CCD sequence time versus CF or recovery was created. Finally, in ad-

dition to the concentration-based CF estimations, a similar CF appraisal based on EC measurements was performed as well.

$$R = 1 - \frac{1}{CF} \tag{3.1}$$

3.3.3. Scaling tests

The cornerstone of the current research work comprised the investigation of potential scaling occurrence on the membrane surface under certain tested conditions. To that end, filtration experiments were performed in order to evaluate the current CCRO desalination systems' resilience against inorganic fouling, when silica-rich feed water was treated, aiming concurrently at a high recovery grade. The synthetic feed solutions contained as high silica concentration as 120 mg/L, thus already at the level of its solubility limit, at roughly neutral pH and at ambient temperature. Moreover, a moderate magnesium quantity of nominal concentration 24 mg/L (1 mM) was included in the feed. Due to the reagents used for the creation of the feed solutions as well as the pH regulation (see Section 3.4), Na^+ and Cl^+ were also present. The exact composition of the synthetic feed solutions is provided in Table C.1 of Appendix C. The co-existence of supersaturated silica with magnesium cations, which as explained in Section 2.2.2 facilitates silica precipitation, rendered the treatment of this particular water a challenging task. The challenge became even greater due to the non-usage of dedicated antiscalant as well as due to the high targeted recovery.

Two distinct experimental series were performed on the basis of different applied CCD sequence duration, translating into different recovery grades. The examined CCD operation times were 20 min and 40 min for the two series, respectively, whereas this selection was based on the results acquired from the recovery determination tests (see Section 3.3.2). Ten sequences of the former and thirty sequences of the latter were performed. It is also noted that 5 sequences out of the thirty, having a CCD duration of 40 min, were performed in the absence of Mg^{2+} in the feed solution in order to examine the effect of magnesium on silica polymerization.

The required data for the analysis of the potential silica scaling were collected throughout each CCD sequence run, as was explicitly described in Section 3.2.2. The data processing resulted in the creation of graphs illustrating the MTC variation over CCD sequence time, from which scaling occurrence could be deduced. MTC values were calculated according to Equation (2.10). Also, from Equation (2.15) the corrected flux was estimated. Regarding TMP values, they were directly retrieved from the pressure gauges readings, whereas $\Delta\pi$ values were implicitly inferred through the EC and temperature readings. More precisely, osmotic pressures were calculated by means of conversion factors used to covert EC (μS/cm) to TDS (mg/L) and finally TDS to π (kPa) values [36]. In its turn, conversion factors calculation was based on the salts concentration, which at any given moment were estimated by the combination of their initial known concentration and the CF. Based on the EC readings of the fresh feed ($EC_{f,fresh}$), permeate (EC_p) and concentrate (EC_c) the CF could be calculated according to Equation (3.2). The derivation of this expression was based on the combination of a salt mass balance with Equation (3.1).

$$CF = \frac{EC_c - EC_p}{EC_{f,fresh} - EC_p} \tag{3.2}$$

In addition to the monitoring of scaling via the MTC, silica mass balance calculations for each sequence were carried out as well. It was theorized that by comparing the final measured silica concentration at the end of each sequence with the theoretically expected final concentration, based on the CF estimation, a deduction about polymerization rate as well as scaling potential could be drawn. This is because a potential deviation between the expected and the measured value would point the extent of the undergone silica polymerization as well as could also indicate retention of silica in the system (in the form of scale on the membrane surface). To that end, a sample was collected from the brine at the end of each sequence and it was analysed for its reactive silica content, by means of the silicomolybdate method. As far as the expected values are concerned, they were calculated from the initial (measured) silica concentrations and the estimated CF (computed according to Equation (3.2)). Calculated and measured concentrations were subsequently plotted on a common graph as functions of the elapsed sequence time. Finally, the fate of magnesium cations inside the CCRO loop was investigated as well. Accordingly, some of the collected final brine samples were also analysed for their Mg^{2+} content. This

knowledge would presumably shed light on the Mg^{2+} contribution to the polymerization process and to the potential enlargement of the scaling risk.

3.4. Chemical solutions

The reagent used as silica source was sodium metasilicate nonahydrate ($Na_2SiO_3.9H_2O$, ≥98% Sigma-Aldrich). In general, sodium silicates are well soluble in water, giving basic solutions. Commercial sodium silicates are produced in ratios of SiO_2:Na_2O ranging from 3.22 to 1 and they consist of three components, namely silica, alkali and water [37]. After their dissolution in water, the resulted solution pH normally ranges from approximately 10 up to 13. Sodium oxide (Na_2O) dissolution reaction, explaining the pH rise, is described by the chemical Equation (3.3).

$$Na_2O + H_2O \longrightarrow 2NaOH \tag{3.3}$$

The required Ca(II) and Mg(II) solutions were prepared using the reagents calcium chloride dihydrate ($CaCl_2.2H_2O$, ≥99% Sigma-Aldrich) and anhydrous magnesium chloride ($MgCl_2$, ≥98% Sigma-Aldrich), respectively. Anhydrous magnesium sulfate ($MgSO_4$, ≥99.5% Sigma-Aldrich) was employed for the recovery determination tests. All of the aforementioned reagents were available in powder form and therefore the desired final solutions were constructed by dissolution of the appropriate salt amounts in deionized water.

As far as the pH regulation is concerned, it was primarily realized by means of hydrochloric acid solution (HCl, 2N Sigma-Aldrich) and when necessary by means of sodium hydroxide solution ($NaOH$, 1N Sigma-Aldrich).

3.5. Analytical methods

In both the CCRO as well as batch experiments the determination of silica concentration comprised an essential part of the analysis. Silica measurements in the current research work were entirely based on the silicomolybdate method. In particular, the Hach Powder Pillow 8185 method was followed, employing the Hach-Lange spectrophotometer DR 3900. According to this method, reactive silica and phosphate react with molybdate ions within an acidic environment, resulting in the formation of yellow-coloured complexes. The citric acid addition eliminates the phosphomolybdic acid complexes and thus the intensity of the remaining yellow colour corresponds to the SiO_2 concentration. With the silicomolybdate method the reactive portion of total silica can be measured, which primarily entails monomeric silica. In most cases, samples needed to be diluted with deionized water before the analysis, because the spectrophotometer's maximum measuring limit was 100 mg/L.

In some experiments hardness ions concentration should be estimated as well. This was performed by means of the ion-exchange chromatography (IC). Previous to the analysis, standard solutions of the targeted ions should be prepared. Since the ion chromatograph analytical limit was up to 100 mg/L, the respective prepared concentrations were 1, 10, 50 and 100 mg/L, covering in that way the whole analytical spectrum. In cases where high ion concentrations were expected, collected samples needed to be first adequately diluted with ultrapure water, so as to fall within the IC measuring range.

4

Results

4.1. Batch tests results

4.1.1. Pure silica solutions

The outcome of the batch tests containing pure silica solutions without pH adjustment are presented in Figure 4.1. The initial SiO_2 concentrations in the various batches ranged from 350 to 1180 mg/L. As can be seen, reactive silica concentration displayed a similar pattern in all cases throughout the 4 hours of the experimental run, namely an initial slight drop within the first ten minutes of the run followed by a nearly constant trend. It is noted, that the deviation between the initial SiO_2 quantity and the rest concentration values could partially emerge from the different ways that those were measured, since the former was estimated by the weighted silica amount dissolved in demi water, whereas the latter was measured by means of the silicomolybdate method. This also applies to all subsequent graphs presented in this chapter. In any case, although the apparent initial drop appears to be somewhat larger at higher supersaturation levels, an extensive monosilicic acid stability was generally observed throughout the examined batch duration. This fact can be attributed to the high pH values prevailed in the batches. In particular, since no pH regulation took place, the solutions' pHs ranged between 11.7 and 12. Under those alkaline conditions, silica solubility rapidly increases due to the electrostatic repulsion among the predominant ionic species (as has been illustrated in Figure 2.4). Overall, it can be concluded that the existing basic conditions in all the investigated batches rendered the reactive monomeric units particularly stable, despite the high supersaturation levels of the pure silica solutions.

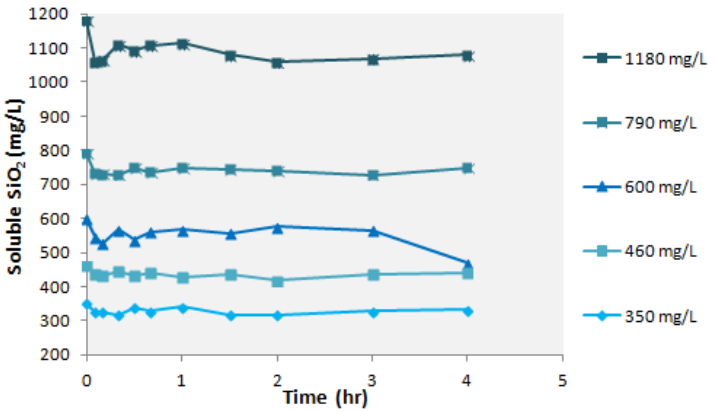

Figure 4.1: Soluble silica concentration over time in the various tested batches. In the legend the initial SiO_2 concentrations of each batch solution are given.

4.1.2. Silica/Ca^{2+} solutions

The soluble silica concentration variations over time, when calcium chloride was added in the solutions, are shown in Figure 4.2. The initial concentrations of both SiO_2 and Ca^{2+} in each of the prepared solutions are provided in the legend. It is obvious, that the preexisted stability of the monomeric units was significantly disturbed by the presence of Ca^{2+} cations. This fact becomes evident by the immediate sharp decline in the monomers concentration directly from the beginning of the experiments. Particularly, both the initially 350 mg/L and 460 mg/L solutions followed roughly identical routes and stabilized to a value close to 200 mg/L, after which a mild gradual decline was carried on until the end of the test. In the same way, the pseudo-stabilization concentration of the initially 600 mg/L sample was approximately 300 mg/L. For comparison purposes, the respective pure silica solution curve (initially 600 mg/L) has been also included in the graph, denoted by the black dashed curve. In this case, silica concentration was maintained for almost the entire run duration above 500 mg/L. It is also noteworthy that differences in the characteristics between pure silica and silica/Ca^{2+} solutions were discernible even to the naked eye. More specifically, in the former case solutions were visually clear, whereas when Ca^{2+} was added they turned instantaneously to cloudy, indicating particles' formation.

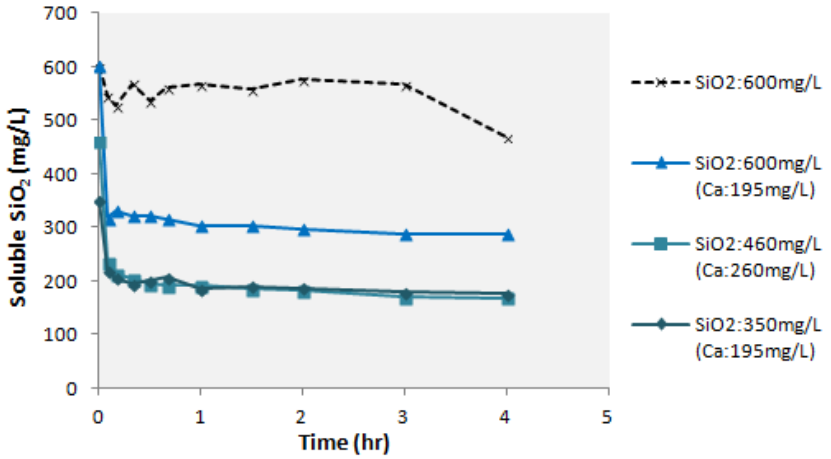

Figure 4.2: Soluble silica concentration over time in the presence of Ca^{2+} cations.

The part of silica that was no longer detectable by the silicomolybdate method was converted to a different form, other than silic acid. In order to shed light on the contribution of calcium cations to the monomeric transformation, Ca^{2+} concentration change over time was also monitored for a particular batch run. The obtained results are shown in Figure 4.3. It appears that along with the initial steep drop in monomeric silica concentration, an important drop in the concentration of calcium took place as well. The solution's pH in this case was about 11.5, thus the vast majority of silica monomers were ionized. Therefore, it can be deduced that the formed precipitate consisted of calcium silicates created either by direct electrostatic attraction of the silicate anions with the Ca^{2+} cations or by co-precipitation of silica with $Ca(OH)_2$ or $CaCO_3$, in case that CO_2 was present in solution. Hence, the general inference stemming from the above observations is that the depletion of silica monomeric units from a highly alkaline solution in the presence of Ca^{2+} ions, does not proceed via the polymerization process but rather through co-precipitation with the instantaneously formed $Ca(OH)_2$ flocks.

4.1.3. Silica/Mg^{2+} solutions

The generated graph concerning the silica/Mg^{2+} solutions is demonstrated in Figure 4.4, in which the Mg^{2+} concentration variation over time (in the batch with initial silica concentration 350 mg/L) has been introduced as well. The general trend in this case exhibits many similarities to the calcium solutions, in the sense that an immediate silica as well as a simultaneous magnesium drop occurred within the first few minutes of the run. However, in this case the decline was more rapid, since soluble silica dropped to approximately 100 mg/L, while magnesium ions were almost eliminated from the solution. The pH values in all batches ranged from 10.4 to 10.7. The shape of the curves depicted in Figure 4.4, along with the instantaneously developed turbidity in the prepared solutions after Mg^{2+} addition, revealed an

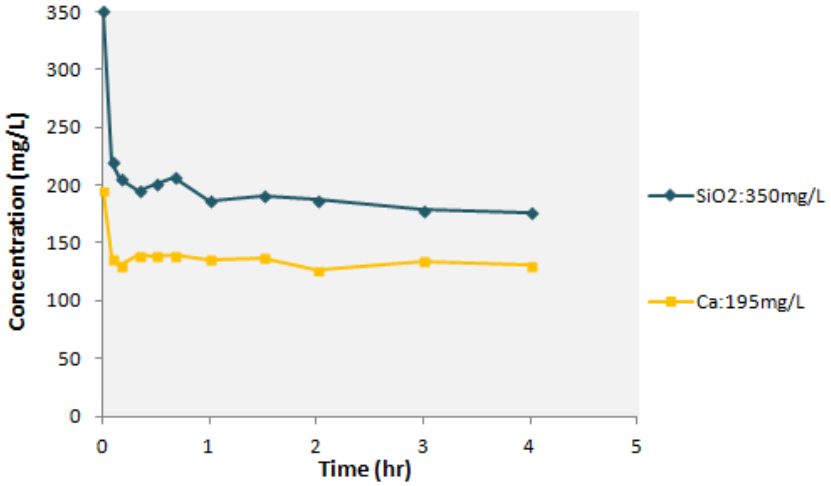

Figure 4.3: Soluble silica and Ca^{2+} concentrations over time for a particular batch test.

immediate particulates formation. It was assumed that in this alkaline medium the produced precipitate contained a mixture of magnesium silicates along with magnesium hydroxide molecules. In their research Nesterchuk and Makarova [38], who chemically analyzed the voluminous white precipitate obtained after mixing magnesium chloride with sodium metasilicate solutions, suggested that the precipitate composition could be described by the chemical formula $MgO{\cdot}1.1SiO_2{\cdot}2H_2O$, which existed in an amorphous state. To summarize, under alkaline conditions the presence of Mg^{2+} cations can instantaneously and dramatically disrupt monomeric silica stability and directly trigger the formation of magnesium silicate precipitates.

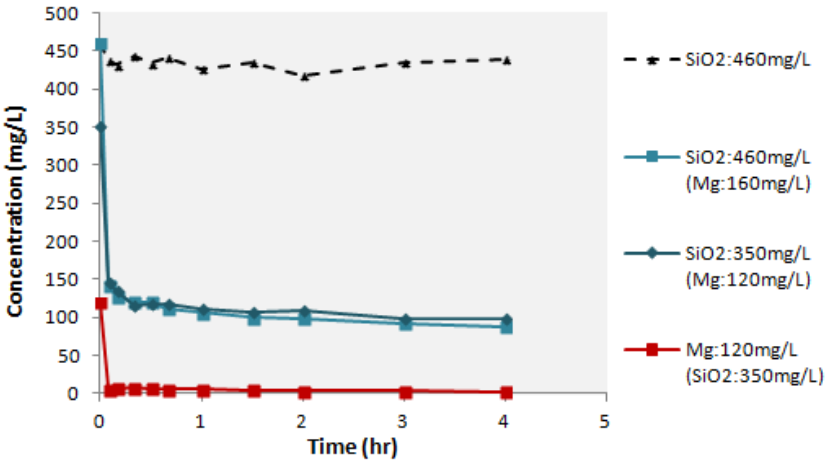

Figure 4.4: Soluble silica and Mg^{2+} concentrations over batch time. The Mg^{2+} concentration variation (red curve) refers to the batch with initial silica 350 mg/L.

4.1.4. Silica/Ca^{2+}/Mg^{2+} solutions

Figure 4.5 depicts concentration changes over experimental time of reactive silica, calcium and magnesium, when both hardness ions were collectively present in the batch solution. The graph of Figure 4.5 represents the examined solution having the following initial composition: 350 mg/L SiO_2, 195 mg/L Ca^{2+} and 120 mg/L Mg^{2+}. The solution pH in this case was 10.2. It is observed that the decrease in the quantity of soluble silica was large and even greater than with any of the two cations separately, reaching a final concentration of roughly 40 mg/L towards the end of the run, a value well below its solubility limit at the given pH. Regarding magnesium cations, they were again almost entirely disappeared from the solution, whereas calcium concentration was also somewhat reduced, yet not in the

same degree as in the batch in which Mg^{2+} was absent (see Figure 4.3). More thoroughly, the final calcium concentration in the common Ca^{2+}/Mg^{2+} solution was roughly 40 mg/L higher as compared with the batch containing only calcium. Overall, it appears that the concomitant presence of both hardness cations induced a more rapid decline of monosilicic acid in the solution, than in the cases where each of the cations participated individually.

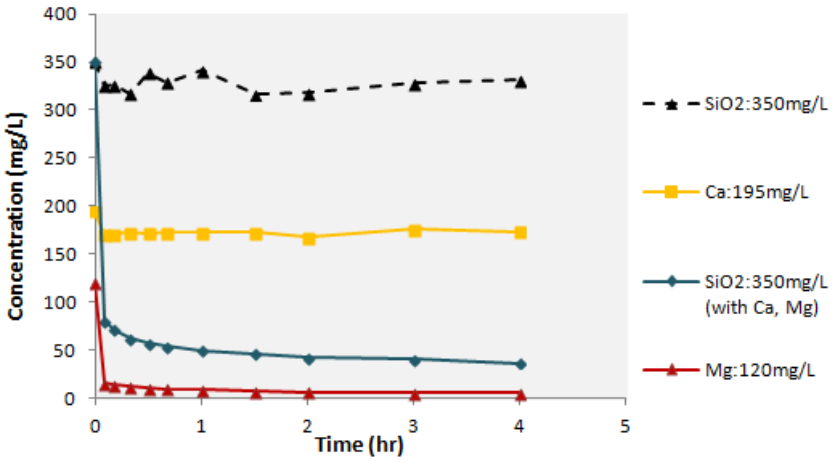

Figure 4.5: Soluble silica, Ca^{2+} and Mg^{2+} concentrations over batch time. The black dashed curve refers to a pure silica solution, whereas the three solid curves refer to the same solution with the quantity of each constituent indicated in the legend.

4.1.5. Effect of neutral pH

The results of the batch tests presented in the previous section concerned pH conditions above 10, since no pH adjustment took place. Unambiguously, this highly alkaline environment vigorously promoted particles generation and precipitation in the form of magnesium and calcium silicates, when hardness cations were part of the solution. Nevertheless, those conditions typically would not be encountered in real conventional RO or CCRO applications. A more common circumstance would be an operation at considerably lower pH. Therefore, in this section the previously obtained results are contrasted with batch tests results performed at near neutral (~7) pH values. The required data were received either from supplementary batch runs performed by the author or from bibliographic resources.

In Figure 4.6, the effect of neutral pH on pure silica solutions is illustrated. The reddish dashed curves correspond to soluble silica concentration changes over time, from batch trials performed at pH 7 by Kempter et al. [4]. The total duration of each of those runs was 62 hours, however here only the first 4 hours are included for the sake of straight comparison with the conducted high pH experiments. According to the graph, up to an initial concentration of about 400 mg/L reactive silica remains stable in solution for the examined duration. On the other hand, this is not the case for an initial SiO_2 concentration of 500 mg/L, where after 3 hours a prompt polymerization and particle formation initiates. This shift towards monomeric destabilization after 3 hours becomes more evident in the original graph provided in Appendix D.1. Finally, in the case of 750 mg/L initial silica, the polymerization of monomeric units and the subsequent particle development and growth can be observed straight from the beginning of the run.

The above results were verified in the context of the same research [4] by means of light scattering measurements as well, which also enabled more precise nucleation induction time estimations of the examined supersaturated solutions. Nucleation induction time is defined as the time delay until stable crystals under supersaturated conditions are formed, which becomes shorter with increasing supersaturation levels. For the examined solutions, the induction time of 400 mg/L initial silica was estimated to about 8 hours, whereas of 500 mg/L to approximately 3 hours (when looking at Figure 4.6, this time essentially comprises the beginning of the rapid drop of the reactive silica concentration). Lastly, in the case of the 750 mg/L SiO_2 batch no actual induction time was observed, since polymerization and particle formation were virtually instantaneous.

Similarly to the alkaline conditions, batch runs were also performed at neutral pH focusing on the effect of hardness ions on silica polymerization. Figure 4.7 shows concentration variations for three

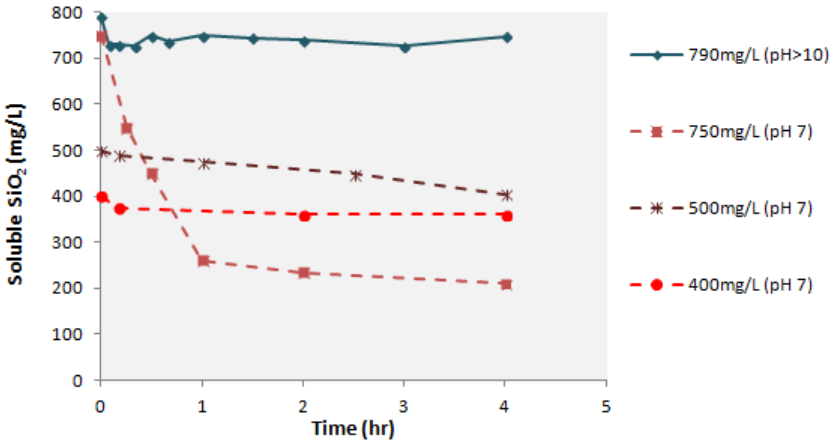

Figure 4.6: Soluble silica concentration over batch time at pH 7 (dashed curves) and at pH > 10 (solid curve). The data regarding pH 7 runs were received from [4].

solutions containing magnesium cations and having initial silica quantities 350, 460 and 600 mg/L, respectively. The solution with the lowest initial SiO_2 concentration appeared generally stable in contrast to the other two, in which polymerization reaction begun promptly. Unsurprisingly, initial higher supersaturation level (600 mg/L) resulted in a more rapid and less gradual soluble silica reduction than lower supersaturation (460 mg/L), however after 3 hours the concentrations in both solutions seemed to converge. By comparing this graph with the one of Figure 4.6, the conclusion can be drawn that Mg^{2+} ions effectively accelerate silica polymerization process. Additionally, the IC analysis performed for a specific batch showed that Mg^{2+} concentration remained unaltered throughout the experimental period (red curve in Figure 4.7), revealing in that way an accelerating effect of Mg^{2+} cations rather than their active participation in the reaction of polymerization. Moreover, analogous conclusions could be drawn for the influence of Ca^{2+} as well, as demonstrates the graph of Figure 4.8. The relatively sharp drop of soluble silica in the solution with initially 460 mg/L SiO_2 along with the steady calcium concentration of 260 mg/L throughout the run, confirmed the role of Ca^{2+} in accelerating silica polymerization rate. In Figure 4.8, the respective soluble SiO_2 curve when Mg^{2+} was present has been included as well. The comparison of the two curves reveals a similar effect of both hardness ions, while the somewhat greater impact of Ca^{2+} appearing in the graph for a limited time interval could be attributed to the marginally higher quantity of calcium (than magnesium) in the solution.

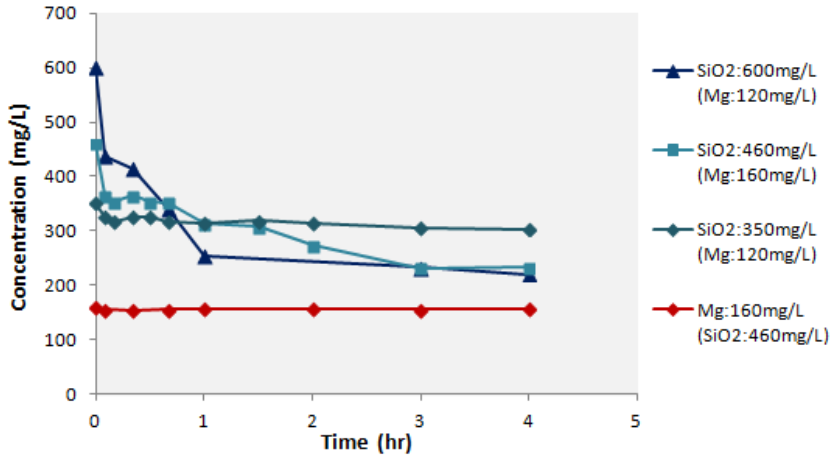

Figure 4.7: Soluble silica concentration (blue curves) over experimental time at pH 7. The red curve corresponds to Mg^{2+} concentration over time in the solution with initial SiO_2 460 mg/L.

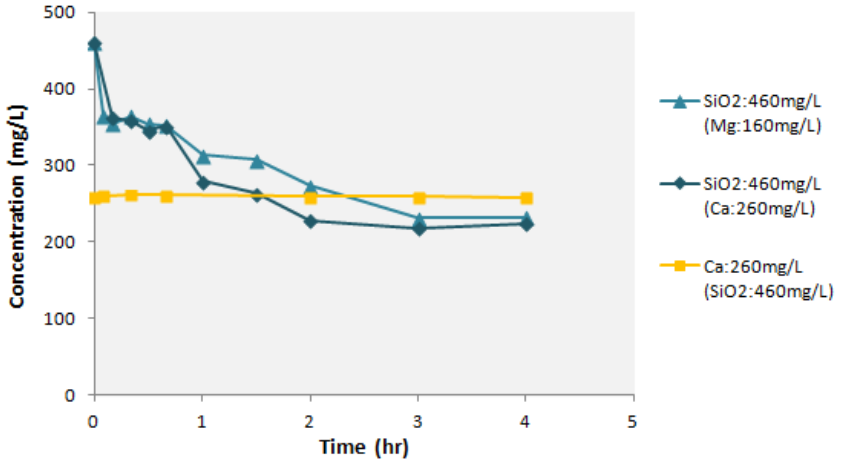

Figure 4.8: Soluble silica and Ca^{2+} concentration variations over time at pH 7 for the solution with initial composition: SiO_2 460 mg/L and 260 mg/L Ca^{2+}. For comparison, silica concentration of the respective SiO_2/Mg^{2+} solution is also given.

4.1.6. Overview of the batch tests results

The aim of the prepared batches was the simulation of potential CCRO brines with main focus on silica investigation. Therefore, the solutions were examined in the light of the silica state throughout the experimental time. The batch tests were performed at ambient temperature under two distinct pH conditions, namely alkaline (pH>10) and neutral (pH∼7) conditions.

The comparative effect of all investigated compositions on the stability of monomeric silica at pH values higher than 10 is schematized in Figure 4.9. In this graph, the reactive silica concentration in the different batches as function of the run time is presented, having an initial value of 350 mg/L. Regarding the pure silica solutions, no significant polymerization occurred even at considerably high supersaturation levels, owing to the great silica solubility at highly alkaline conditions, as a result of the electrostatic repulsion among the predominant silicate anions. Nevertheless, in the presence of hardness cations the apparent reactive silica stability was dramatically disturbed and monomers concentration immediately reduced. The IC analysis revealed a concurrent Mg^{2+} and/or Ca^{2+} concentration decline, which indicated the creation of insoluble magnesium- and calcium- silicates as well as the silicate anions adsorption onto Mg^{2+}- and Ca^{2+} hydroxides as the key mechanisms leading to the rapid monomeric silica reduction. The formation of precipitates was instantaneous after hardness addition. What is more, Figure 4.9 shows the relatively higher effect of Mg^{2+} to react with as well as to adsorb monosilicic acid at the given conditions as compared to Ca^{2+}. Lastly, the co-existence of both hardness cations in the solution stimulated quicker soluble silica drop in comparison to each of them separately. However, most probably this might be merely the result of the higher total hardness quantity present in the former case than in the latter.

The more commonly encountered situation of near neutral pH conditions was examined as well. The summarized graph of the conducted runs at pH 7 is presented in Figure 4.10. Pure silica solutions exhibited significant stability for the examined 4-hour duration up to a 3.3 fold supersaturation level (400 mg/L), however from about 4.2 fold supersaturation (500 mg/L) and beyond this apparent stability was disrupted and polymerization begun. Especially, in cases of particularly high supersaturation levels (e.g. initial 750 mg/L SiO_2) the polymerization process started instantaneously, without considerable induction delay. As far as the effect of hardness cations is concerned, they played an important role in monomeric silica depletion, yet not as profound as under basic conditions. For instance, as Figure 4.7 shows, silica concentration remained steady when its initial value was 350 mg/L, despite the presence of 120 mg/L Mg^{2+}. However, the situation changed drastically with an initial SiO_2 concentration of 460 mg/L and in the presence of either 160 mg/L Mg^{2+} or 260 mg/L Ca^{2+}, in which cases the polymerization process begun expeditiously. If hardness ions would not be part of the solution, soluble silica stability would be greater, as the curve corresponding to initial silica 500 mg/L clearly shows. Finally, the IC analysis exhibited unaltered hardness concentrations in cases where SiO_2 monomers were reduced, denoting the effect of divalent cations to accelerate silica polymerization process, but without being actively involved in the reaction. Naturally, hardness influence weakens at higher supersaturation levels,

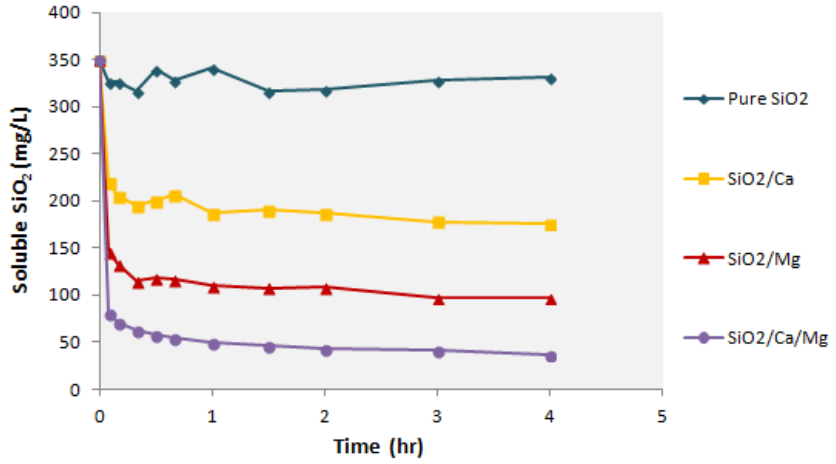

Figure 4.9: Comparative graph of soluble silica concentrations over time for the various examined batches at pH above 10. In all batches the initial SiO_2 concentration was 350 mg/L. Whenever Ca^{2+} and/or Mg^{2+} were preset their concentration was 195 mg/L and 120 mg/L, respectively.

since monomeric silica polymerization would occur rapidly anyway.

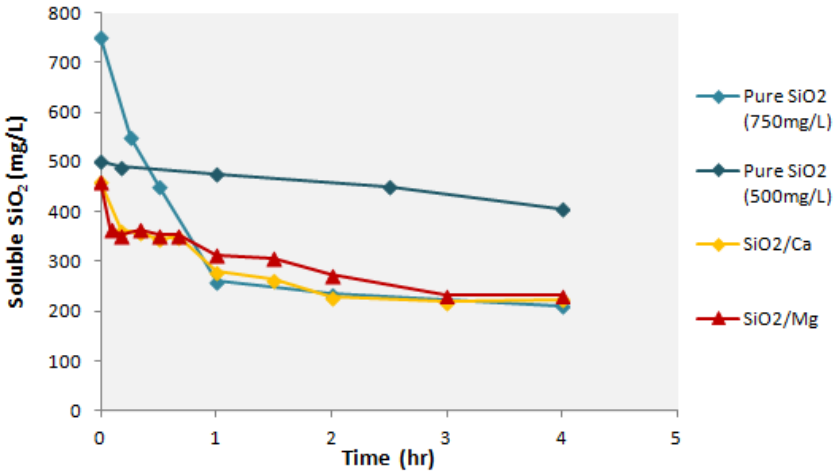

Figure 4.10: Comparative graph of soluble silica concentrations over time for the various examined batches at pH 7. In the SiO_2/Ca^{2+} solution the concentrations were 460 and 260 mg/L, respectively, whereas in the SiO_2/Mg^{2+} solution the concentrations were 460 and 160 mg/L, respectively.

4.2. Preliminary filtration tests

4.2.1. Pristine membrane water permeability

The determination of the pristine membrane water permeability was realized via a filtration test in PFD mode and at an ambient temperature of about 18.5°C. Since ion-free pure water served as feed, the result would be similar in case that the test would be carried out in CCD mode. The obtained results are presented in Figure 4.11. According to them, a relatively significant influence of the flux variations on the MTC value could be observed. More specifically, the MTC faced a drop of roughly 25% when the flux was doubled. For this reason, the MTC value corresponding to a 15 L/m^2 h flux was considered as the clean membrane water permeability rather than the curve slope. This is because this specific permeate flux was the one applied during the CCRO scaling tests. Eventually, the MTC of the pristine membrane was calculated to be 4.95 L/m^2 h bar or $1.37 \cdot 10^{-8}$ m/s kPa.

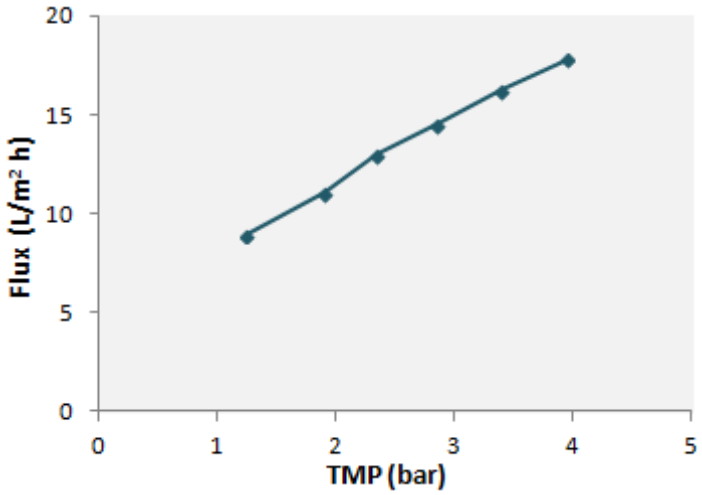

Figure 4.11: Permeate flux as function of different applied TMPs.

4.2.2. Recovery determination over time

Two individual experimental trials were performed to determine the recovery of the system as function of the sequence time. In the first one Mg^{2+} concentration while in the second one SO_4^{2-} concentration were measured. In each case, the rejection of both ions should be identical, despite the negative surface charge of the BW30-4040 element, due to the electrical neutrality maintenance principle. The experimental duration was 1 hr for each of the filtration tests, whereas a sampling frequency of 20 min was applied. The produced graph concerning the test measuring sulfate concentration over time is depicted in Figure 4.12. Based on this, the required duration for a specific recovery to be reached could be determined. Furthermore, in addition to the concentration-based estimations, the filtration run was repeated focusing on the electrical conductivity measurements of the recycled brine, as this method was also followed during CCRO tests in order to estimate the recovery at any given moment. The summarized results of both filtration tests along with the LewaPlus projections are presented in Table 4.1. Based on those values, the proper CCD sequence time for the scaling tests was chosen. Thus, aiming at roughly 80% and 90% recoveries, sequence times of 20 min and 40 min, respectively, were selected.

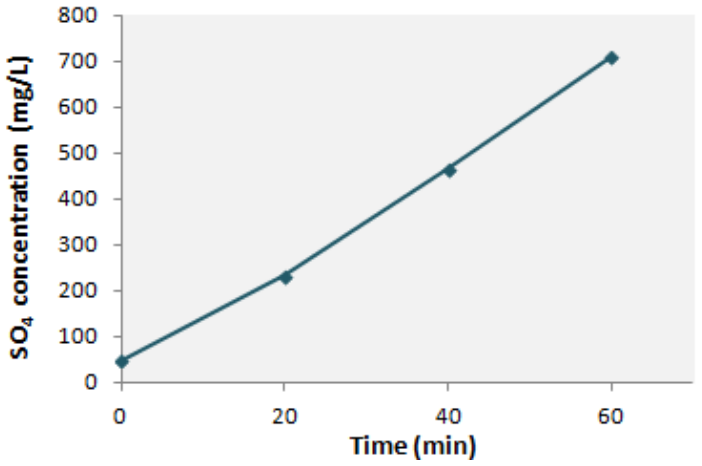

Figure 4.12: Sulfate concentration in the recycled brine at different time points.

Table 4.1: Concentration factors and recoveries versus elapsed times in the various trials.

	Test 1	**Test 2**		**LewaPlus**
Measured quantity	*Mg concentr.*	*SO_4 concentr.*	*EC value*	-
Elapsed time (min)	**CF (R)**	**CF (R)**	**CF (R)**	**CF (R)**
20	4.45 (77.5%)	4.91 (79.6%)	4.82 (79.3%)	6.07 (83.5%)
40	8.14 (87.7%)	9.86 (89.8%)	8.60 (88.4%)	10.64 (90.6%)
60	13.91 (92.8%)	14.90 (93.3%)	11.30 (91.2%)	15.38 (93.5%)

4.3. CCRO scaling tests

In this section the results regarding the CCRO scaling experiments are manifested. Those involved tests with either 20 min or 40 min sequence time. A total of 40 sequences were performed in sets of 5 in a row, meaning that after 5 sequences a new feed solution needed to be prepared for the next 5 sequences and so forth. Therefore, the following results are presented in graphs of 5 sequences sharing the same feed solution. In all cases, experiments took place at ambient temperature and under near neutral pH conditions, at constant flux of about 15 L/m^{2}h (lmh), while having the nominal feed composition of 120 mg/L SiO_2 and 24 mg/L Mg^{2+}, except for the last 5 sequences in which magnesium was excluded from the prepared solution.

4.3.1. CCRO scaling tests: 20 min sequence time

In order to identify whether scaling took place during the filtration process two factors were primarily monitored, namely the MTC and the applied pressure provided by the feed pump. A noticeable drop of the MTC and/or a substantial increase of the P_{feed} would attest potential scaling occurrence. Therefore, those two parameters are illustrated in the following graphs as functions of the operation time.

The results for the first five sequences carried out consecutively are given in Figure 4.13. The pH of the feed solution was 7.1. The MTC values ranged between $1.18 \cdot 10^{-8}$ and $1.32 \cdot 10^{-8}$ m/s kPa having an average value of $1.27 \cdot 10^{-8}$ m/s kPa. It is reminded that the respective pristine membrane permeability was $1.37 \cdot 10^{-8}$ m/s kPa. As far as the schematic of the applied pressure is concerned, it comprises a typical representation of P_{feed} progression throughout a CCRO operation, during which P_{feed} gradually rises following the osmotic pressure increase while reaching its maximum value at the end of each sequence, before it drops again to its initial minimum value after the brine discharge and the flushing of the system. In the current graph as well as in the graphs to follow, the first P_{feed} point noted in the curve of each new sequence corresponds to the measured value after five minutes of the sequence start and not straight in the beginning of it, allowing for a system's stabilization period to elapse.

As can be seen, the MTC curve displays a generally zero slope trend translating into an average steady MTC value. In the graph, as well as in the graphs to follow, the trendline of the MTC values together with the corresponding equation have been included. Also, the maximum as well as the minimum P_{feed} values are roughly identical among all the examined sequences. Hence, the apparent constant MTC value along with the highly repeatable P_{feed} values at specific time points among the various sequences, seem to rule out any possibility of scaling. The obtained recoveries were between 82% and 83.1%, whereas the highest recorded applied pressure was 6.7 bar.

The respective MTC and P_{feed} variation curves for the next five sequences are demonstrated in Figure 4.14. In this case, MTC values were in the range of $1.20 \cdot 10^{-8}$ and $1.26 \cdot 10^{-8}$ m/s kPa with an average value of approximately $1.24 \cdot 10^{-8}$ m/s kPa. Also, the highest applied pressurein this sequences series was 7 bar, whereas the system recovery varied between 82.2% and 83.6%. The prepared feed solution had a pH value of 6.5. In general, a similar conclusion as with the first five sequences can be drawn, which is the absence of scaling on the membrane surface. The roughly unchanged MTC values along with the repeated pressure values throughout the filtration runs justify this deduction.

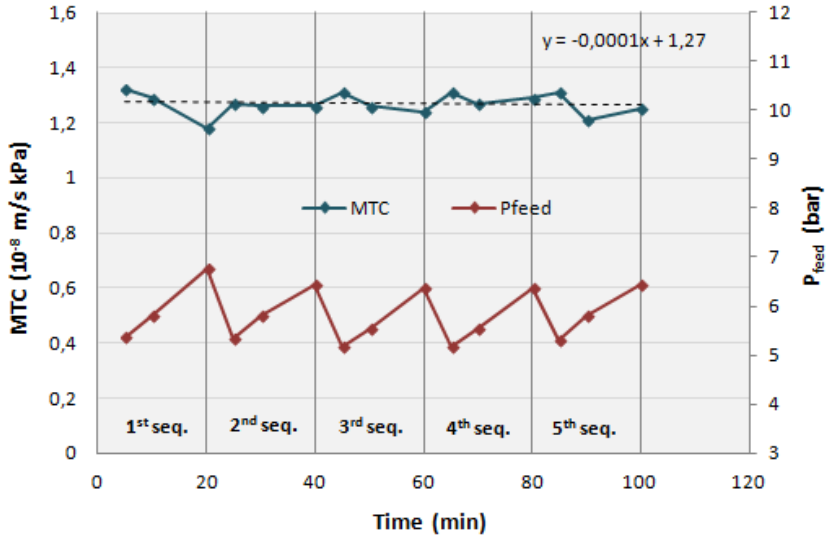

Figure 4.13: MTC and applied P_{feed} variations over time for sequences 1 - 5. Each sequence duration was 20 min.

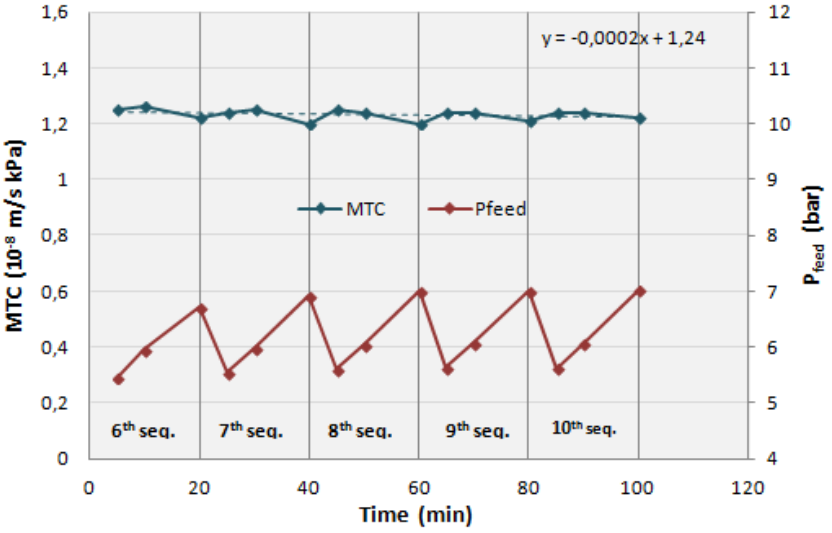

Figure 4.14: MTC and applied P_{feed} variations over time for sequences 6 - 10. Each sequence duration was 20 min.

4.3.2. CCRO scaling tests: 40 min sequence time

The filtration tests described in the previous section referred to sequence duration of 20 min reaching in that way a maximum recovery of 83.6%, without any fouling indication. Aiming at a higher recovery the sequence duration increased to 40 min for the filtration runs to follow. Accordingly, the subsequent figures demonstrate the MTC and P_{feed} curves resulted from sequences carried out under the prolonged sequence time regime.

In Figure 4.15, a roughly identical trend as with the respective 20 min sequence graphs can be observed. This is the relatively unaltered MTC values displaying only minor fluctuations throughout the CCD operation (having a mean value of approximately $1.24 \cdot 10^{-8}$ m/s kPa) as well as the P_{feed} curve showing the same pattern of repetitive values in each of the consecutive sequences. This motif becomes evident by looking at the nearly identical maximum P_{feed} values reached in every sequence. As was expected, the longer CCD runs of the current sequences resulted in higher applied pressures than in the case of the sequences operating at half that time. The maximum applied pressure recorded during the current sequence series was 7.9 bar. Regarding the MTC curve, a slight upward incline can be distinguished (also observed from the MTC trendline slope) which could be attributed to some

variations in the permeate flow rate caused by the feed pump. In particular, towards the end of each sequence somewhat higher Q_p values were observed. Nevertheless, the arisen increased MTC values did not substantially deviate from the mean and as can be seen in Figure 4.16 this upward trend disappeared during the next five sequences. Overall, the conclusion drawn from Figure 4.15 constitutes a scaling-free CCRO operation, achieving high recoveries between 89.9% and 90.9%, which corresponded to final silica concentrations in the brine of about 1190 mg/L to 1310 mg/L. The solution pH was 6.8.

During the next five-sequence series (6 - 10), no signs of scaling were detected as well, as follows from the shape of the curves and the roughly zero trendline slope depicted in Figure 4.16. In this case, the initial pH of the feed was 6.8. Throughout the CCD sequences an average MTC value close to $1.26 \cdot 10^{-8}$ m/s kPa was found, whereas a maximum pressure of 8 bar was recorded. The recovery ranged between 89.6% and 90.7%, which translates into a final silica concentration in the brine between 1150 mg/L and 1293 mg/L.

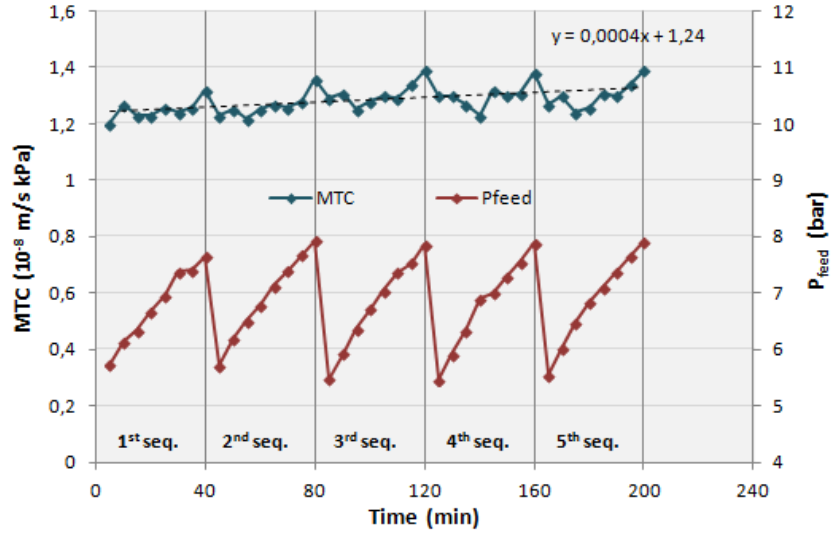

Figure 4.15: MTC and applied P_{feed} variations over time for sequences 1 - 5. Each sequence duration was 40 min.

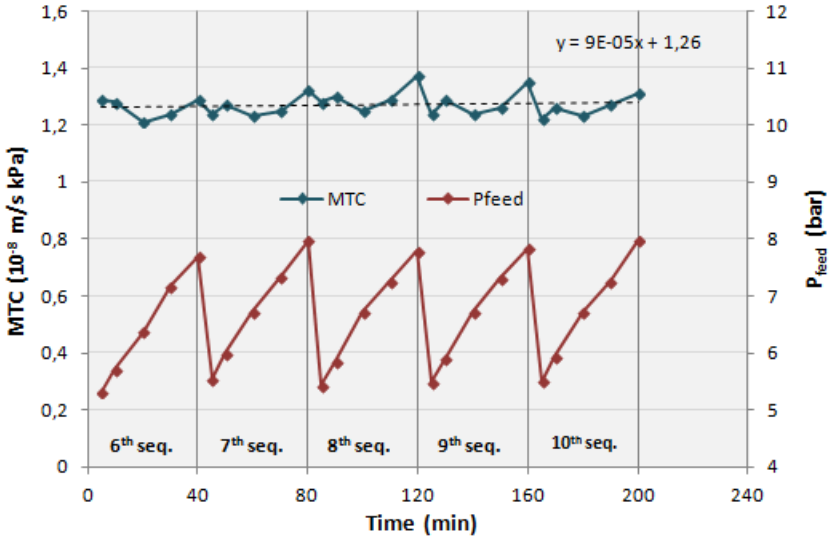

Figure 4.16: MTC and applied P_{feed} variations over time for sequences 6 - 10. Each sequence duration was 40 min.

The emerging results concerning sequences 11 to 15 are demonstrated in Figure 4.17. In this occasion, a slight gradual downward trend of the MTC curve was discernible, especially after the first sequence, which during the CCD runs fluctuated between 1.18 and $1.3 \cdot 10^{-8}$ m/s kPa. The average

MTC value was $1.24 \cdot 10^{-8}$ m/s kPa. Also, a gentle rise of the maximum required P_{feed} occurred during the last three sequences, reaching the top (8 bar) in the last cycle of the final sequence. Despite the fact that those indications might imply the existence of some restricted silica attachment on the membrane surface, yet severe scaling did not occur, otherwise a sudden MTC decline along with a sharp P_{feed} increase would take place. Additionally, a slight downward trend was also observed in some of the previous runs where no scaling took place. Further filtration runs were necessary to elucidate whether the descending trend of permeability would be permanent signifying scaling or if it would have been caused by other reversible factors. It is noted, that in this case the prepared initial feed had a pH of 6.5, while the achieved final recovery ranged between 89.3% and 90.6% among the performed sequences.

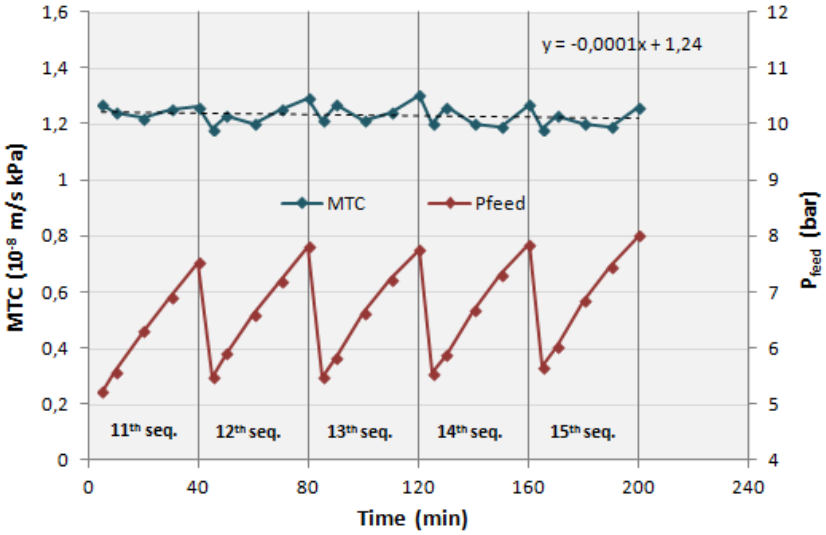

Figure 4.17: MTC and applied P_{feed} variations over time for sequences 11 - 15. Each sequence duration was 40 min.

Subsequently, five additional sequences (16 - 20) were realized with the same feed composition (120 mg/L SiO_2, 24 mg/L Mg^{2+}) having pH 6.8. The resulted MTC and P_{feed} variations over time are schematized in Figure 4.18. At first, the MTC value seemed to be restored during the 16th sequence, however from the 17th one and beyond an important steady MTC drop took place, which coincided with a simultaneous increase in the required applied pressure. Undoubtedly, those observations comprised significant indications of scaling existence on the membrane surface. The MTC towards the end of the 20th sequence dropped to a value close to $1.1 \cdot 10^{-8}$ m/s kPa. As far as the maximum P_{feed} value in the the various sequences is concerned, it begun with 7.2 bar in the 16th sequence and rose up to 7.8 bar in the 20th sequence.

The ultimate proof of scaling occurrence came from the following five sequences (21 - 25), the results of which are shown in Figure 4.19. The pH of the feed was 6.8. In this case, the rapid decline of the MTC as the sequence progressed becomes glaringly obvious. The fact that MTC diminished with every new sequence revealed the inability of the intermediate PFD flushings to recover the previous permeability states, rendering the development of scalants and the consequent membrane surface coverage as the only reasonable explanations for the permeability drop. As expected, MTC reduction was accompanied by a relatively steep increase of the required applied pressure. In particular, from the 21st until the 25th sequence the maximum P_{feed} level rose from 7.5 to 8.8 bar.

Finally, a last series of five sequences (26 - 30) was carried out employing the same already scaled membrane element, aiming at investigating the effect of magnesium ions on the rate of silica scaling. To that purpose, Mg^{2+} was not added in the prepared solution, which in this case contained only 120 mg/L of silica, at pH 6.5. The acquired results are shown in Figure 4.20. The slope of the MTC curve divulged a clear deceleration rate of silica scaling as compared with the previously examined silica-magnesium solutions. Since scaling continued to take place but in a substantially lower rate, it was deduced that the presence of Mg^{2+} ions effectively accelerated silica precipitation rate. This outcome is in full agreement with the results obtained from the batch tests regarding the effect of Mg^{2+} on silica polymerization and precipitation potential.

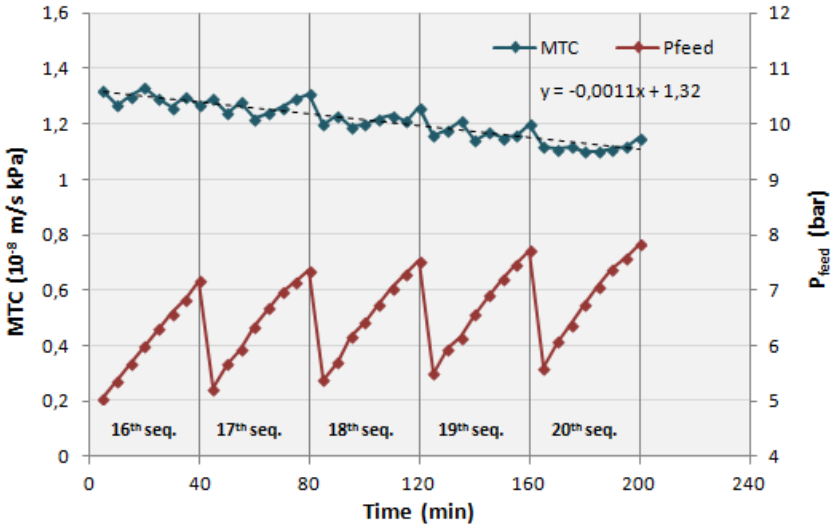

Figure 4.18: MTC and applied P_{feed} variations over time for sequences 16 - 20. Each sequence duration was 40 min.

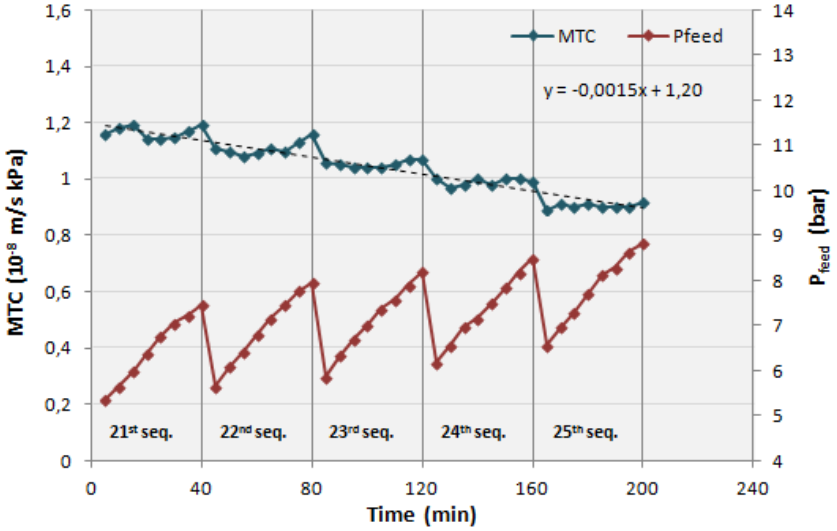

Figure 4.19: MTC and applied P_{feed} variations over time for sequences 21 - 25. Each sequence duration was 40 min.

4.3.3. Soluble silica mass balance

Aiming at monitoring the fate of soluble silica inside the system, a sample of the final brine of each sequence was collected (from the loop just before the PFD initiation) and analysed for its monomeric silica content. The recorded values were then contrasted with the calculated soluble silica concentrations in the brine. The calculated values were based on the initial SiO_2 concentration and the concentration factor. In Figure 4.21, the measured and calculated silica concentrations for sequences 1 to 5 are illustrated. The CCD duration of those sequences was 20 min, reaching a maximum recovery grade of 83.1%. It is obvious that a substantial deviation between measured and calculated values occurred, which signifies a considerable transformation degree from monomeric units into larger polymers. Since no scaling took place during this sequences series, it is theorized that the missing silica quantity (difference between measured and calculated value) was transformed into polymers and/or colloids, which were successfully flushed out at the end of each run by means of the PFD process. Particularly, on average about 60% of total silica had left the monomeric state until the end of the CCD operation. Similar observations were made for sequences 6 to 10 as well, the respective graph of which is provided in Figure E.1 of Appendix E.1. Interestingly enough, the polymerized percentage in this case was only 50.9%. This apparent reduced degree of polymerization could be possibly attributed to the lower pH (6.5) conditions prevailing in the feed solution of this series (leading to lower polymerization rate) as

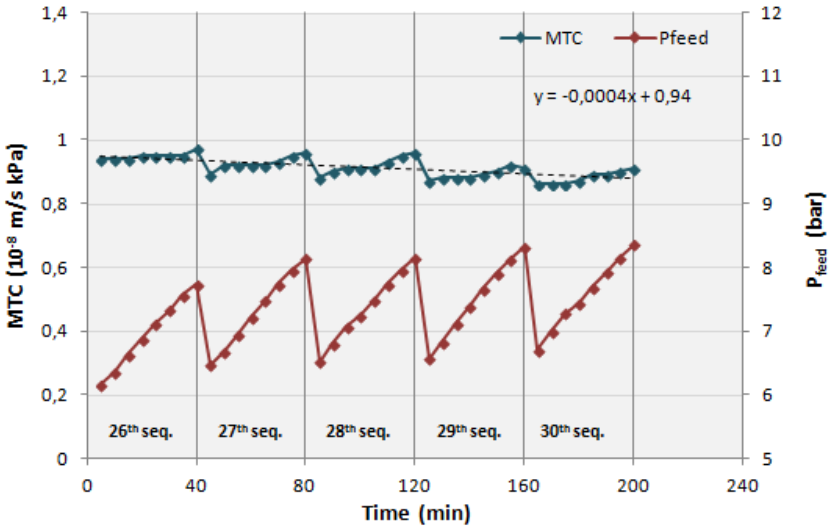

Figure 4.20: MTC and applied P_{feed} variations over time for sequences 26 - 30. The feed solution contained 120 mg/L SiO_2 in the absence of Mg^{2+}. Each sequence duration was 40 min.

compared with the feed solution of the first five sequences, which had a pH value of 7.1.

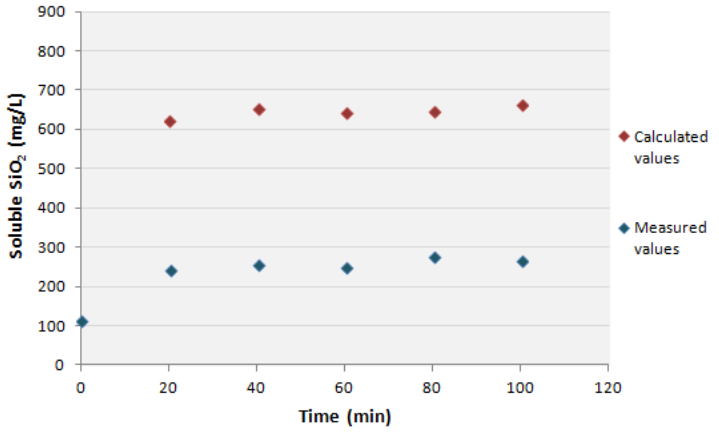

Figure 4.21: Measured and calculated soluble SiO_2 concentration values in the final brine of each 20 min sequence. The depicted values concern sequences 1 - 5.

Analogous graphs comparing measured and calculated reactive SiO_2 concentrations were created for the 40 min sequences as well. In total, fifteen 40 min CCD runs (1 - 15) were performed without important scaling signs, as was described in the previous section. Indicatively, the results for sequences 6 - 10 are presented in Figure 4.22, whereas the corresponding graphs for sequences 1 - 5 and 11 - 15 are available in Appendices E.2 and E.3, respectively. Naturally, in this case of longer runs the calculated final concentration was also higher, due to the larger recovery grade. It is noteworthy, that the measured average final SiO_2 concentration was lower for the 40 min sequences than for the 20 min ones, namely ~230 mg/L and ~300 mg/L, respectively. This means, that the quantity of silica that was not detectable by the silicomolybdate method at the end of the 40 min sequences was roughly 81%. Taking the absence of scaling into consideration, it is inferred that the longer duration of the high recovery sequences was responsible for the larger polymerization extent. Although the additional operational time was relatively short (20 min), this passed under particularly high supersaturation conditions, which evidently made a difference in terms of the induced polymerization rate.

In Figure 4.23, the mass balance comparison outcome is illustrated, for the first five sequences (16 - 20) during which intense scaling was observed. Similar results were received for sequences 21 - 25 as well, which are provided in Appendix E.4. The depletion of silica monomers in those experiments was even more extensive than in the previous 40 min sequences. More specifically, the final SiO_2

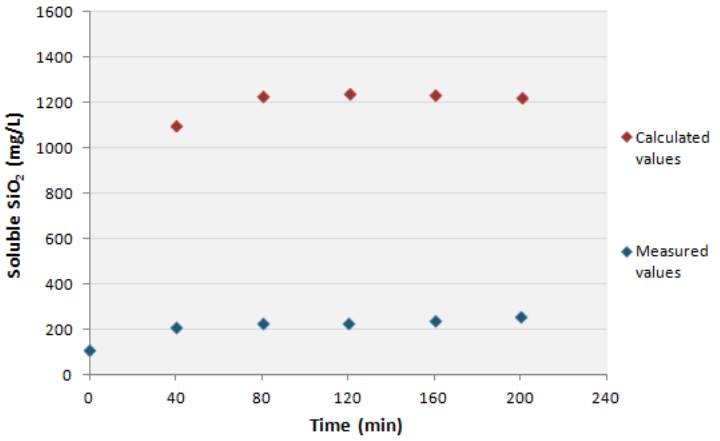

Figure 4.22: Measured and calculated soluble SiO_2 concentration values in the final brine of each 40 min sequence. The depicted values concern sequences 6 - 10.

concentration in the brine was in the range of its solubility limit (approximately 105 mg/L), which signifies that the quantity of reactive silica in the concentrate stream reduced by approximately 91% throughout the process. Presumably, this additional vanishing of reactive silica could be attributed to the monomers attachment onto the already formed scale layer, since otherwise both the operational duration as well as the supersaturation level were comparable in the current runs with the previously conducted ones. Finally, the reactive silica in the concentrate of the sequences 26 - 30, which were performed in the absence of Mg^{2+} cations, was also diminished by an average percentage of 91%. The respective produced graph is shown in Figure E.5 of Appendix E.5.

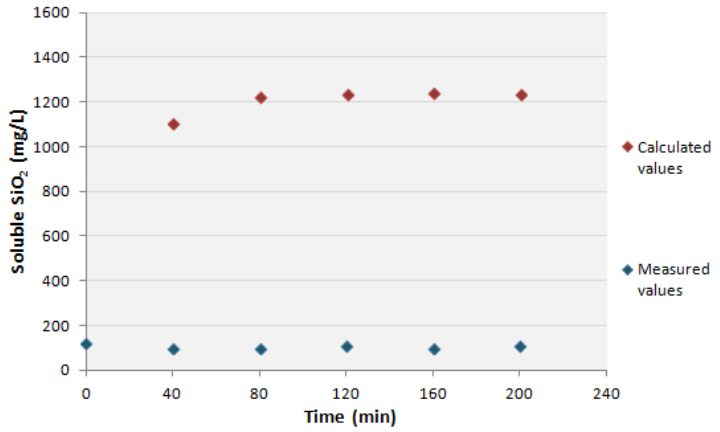

Figure 4.23: Measured and calculated soluble SiO_2 concentration values in the final brine of each 40 min sequence. The depicted values concern sequences 16 - 20.

4.3.4. Magnesium cations mass balance

Complementary to the reactive silica mass balance measurements, the progression of magnesium concentration over time in the CCRO loop was examined, too. Graphs showing the comparison between calculated and measured Mg^{2+} concentrations were created for the sequences (16 - 25), during which severe scaling took place. In Figure 4.24, the resulted graph for sequences 21 - 25 is presented, in which essentially identical calculated and measured Mg^{2+} values can be noticed. In fact, it appears that the measured values were somewhat higher than the calculated ones, which in reality reflects the differences in the methods used for their estimation. Particularly, the measured values were directly received from the IC analysis of the collected samples, while for the calculated values the concentration factor was employed, the estimation of which was based on the electrical conductivity readings. A similar graph was produced for sequences 16 - 20 as well, which is presented in Figure E.6 of Appendix E.6.

The outcome of the indistinguishable values between measured and calculated magnesium concentrations, in fact, suggests that Mg^{2+} total quantity remained dissolved in the brine throughout the entire process and thus it was not part of the formed scale. This result is absolutely in line with the results obtained from the batch tests at neutral pH conditions, where it was revealed that although Mg^{2+} ions facilitated silica polymerization, they did not participate in the formed polymers.

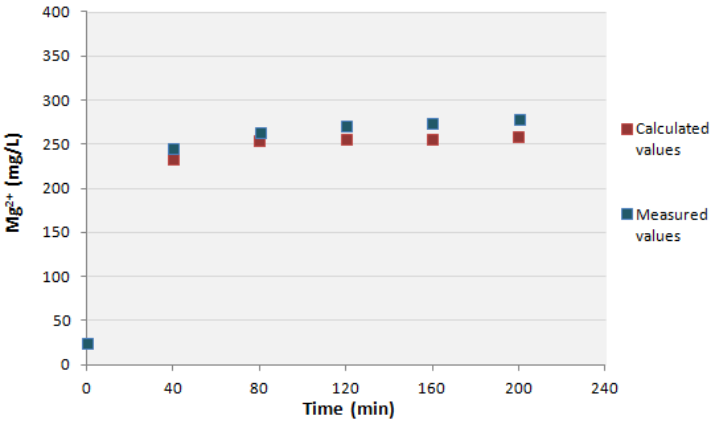

Figure 4.24: Measured and calculated Mg^{2+} concentration values in the final brine of each 40 min sequence. The depicted values concern sequences 21 - 25.

4.3.5. Overview of the filtration tests results

The core subject of the current study comprised the inspection of the CCRO configuration performance in the light of silica scaling retardation potential. For that reason, a campaign of filtration experiments was carried out during which scaling indicators were monitored. All the prepared solutions which served as feed for the CCRO system had a pH value close to 7, whereas all filtration runs were performed at ambient temperature. A nominally constant permeate flux was maintained throughout the entire process, namely 15 lmh.

A total of forty sequences was performed and the overview of the results concerning scaling occurrence is demonstrated in Figure 4.25. The scaling monitoring was realized via the mass transfer coefficient (representing the normalized permeate flux) variations over sequence time. Figure 4.25 shows all the conducted CCD sequences, which for the sake of the current summary graph have been placed consecutively and over the cumulative operational time. The blue data points correspond to experiments with feed solutions having the following composition: 120 mg/L SiO_2 and 24 mg/L Mg^{2+}. The red data points represent the sequences in which a Mg^{2+}-free solution was employed, composed simply of 120 mg/L SiO_2. As can be seen, the blue data points can be further distinguished into light blue and dark blue ones. The former concern sequences of 20 min CCD duration, while the latter of 40 min CCD duration.

The initial ten CCD runs (light blue data points) consisted of sequences lasting 20 minutes each, reaching in that way recovery grades between 82% and 83.6%. Throughout those roughly 3.5 hours of desalination process, MTC remained relatively unchanged displaying an average value of about $1.25 \cdot 10^{-8}$ m/s kPa, thus the possibility of scaling could be ruled out. The subsequent 25 runs (dark blue data points) regarded sequences with CCD duration of 40 minutes each. Focusing on the first fifteen of them, the continuation of a comparatively constant MTC trend was observed. The average MTC value in this 15-sequence series was about $1.25 \cdot 10^{-8}$ m/s kPa, whereas the achieved recovery fluctuated between 89.3% and 90.9%. In this case as well, no indication of scaling could be identified, at least not until the last 4 sequences of this series (thus after $\sim$11 hours of total operation), when a gentle downward trend of the MTC curve appeared. The last ten 40 min CCD sequences begun at 13.4 hours of operation, exhibiting an initial restoration of the MTC value followed by a rapid drop until the end of those runs, at 20 hours of total operation. Undoubtedly, during those final 40 min sequences intense scaling took place. Finally, a last series of 40 min CCD runs was conducted employing the same scaled membrane element, but this time Mg^{2+} was excluded from the prepared feed solution. As can be seen from the red data points in Figure 4.25, the declining tendency of the MTC curve was maintained, yet

the dropping rate was markedly lower than before. This outcome revealed an unambiguous effect of Mg^{2+} ions on accelerating silica precipitation.

The final brine of each sequence was analysed for its soluble silica content targeting at drawing conclusions about the silica polymerization rate. It was found that in every case the majority of total silica in the effluent was not in its monomeric form anymore, denoting that substantial polymerization took place. More thoroughly, the average percentage of total silica that had departed from its monomeric state at the end of the 20 min-, 40 min- without scaling and 40 min- with scaling sequences was 55%, 81% and 91%, respectively. The significant deviation in the apparent polymerization extent between the 20 min and the 40 min sequences clearly stemmed from the difference in the operational duration of the two cases. Interestingly, it was found that roughly 10% less soluble silica existed in the brines of sequences where severe scaling took place as compared to the ones without scaling. Since all the other factors were identical between the two cases, it was assumed that the additional reactive SiO_2 disappearance was owing to the adsorption of monomers onto the colloidal layer already attached on the membrane surface. Lastly, as far as the Mg^{2+}-free sequences are concerned, the percentage of monosilicic acid depletion was also 91%. Again, in this case monomers were adhered to the silica scale coating, up to the point that the thermodynamic solubility limit in the solution was attained (~122 mg/L).

Additionally, the magnesium ions concentration in the final brines of the sequences with important scaling was measured. IC analysis revealed that there was no deficit in the expected (calculated) Mg^{2+} quantity, signifying their non-participation in the formation of the scale deposits.

All in all, the conducted experiments showed an entirely scaling-free operation of a CCRO system for at least 11 hours and without severe scaling indications for about 14 hours, under constantly supersaturated conditions with respect to silica, in the presence of Mg^{2+} cations and in a near neutral pH environment. In particular, throughout the scaling-free desalination process SiO_2 concentration in the loop ranged from 120 mg/L up to about 1320 mg/L, translating into a maximum recovery of 90.9%. What is more, at the end of each sequence the largest part of total silica in the brine was not in a monomeric form, thus rapid polymerization occurred during the concentrate recirculation process. Finally, it was shown that Mg^{2+} cations effectively promoted polymerization process, yet they were not part of the formed fouling depositions. Those deductions completely agreed with the conclusions drawn from the batch experiments.

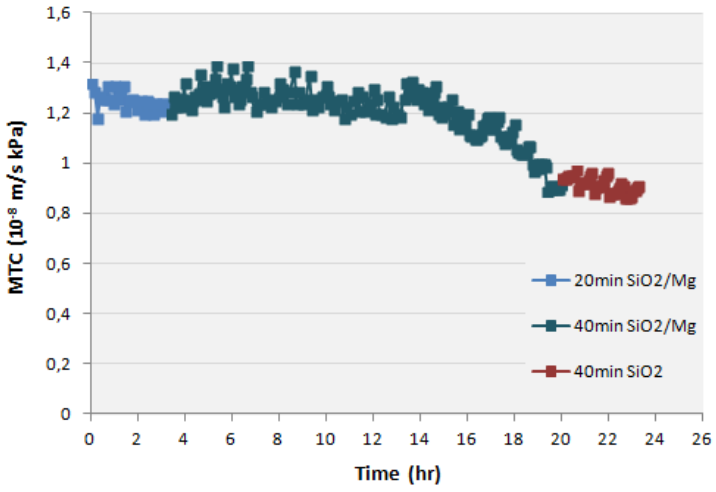

Figure 4.25: Overview of the CCRO tests. The conducted CCD sequences have been placed consecutively over the cumulative CCD operational time.

5

Discussion

5.1. Discussion on the batch tests results

The particularly high stability of silicic acid in pure silica solutions at pH values above 10 provides a solid explanation for the findings of Motchan's study [15], in which no important monomers depletion was observed even at measured silica concentration of the final brine as high as 1800 mg/L. Those CCRO experiments were conducted at initial SiO_2 concentration of 120 mg/L, while the CCD duration of the sequences was either 1 or 3 hours. According to this, it can be predicted that during the treatment of silica-rich feed water under highly alkaline conditions and for the usual operational duration of a single CCD sequence (normally below 1 hour) silica most probably would remain in its monomeric form, even at recovery grades above 90%. Of course, the prerequisite for this to happen is the absence of hardness cations from the feed stream, otherwise precipitates made up of insoluble metal-silicates would be instantaneously formed.

In section 4.1.5, part of the results of Kempter et al. [4] study was presented, regarding batch tests with pure silica solutions at pH 7 focusing on the polymerization rate investigation. Solutions with initial silica concentration levels ranging from 300 to 750 ppm (300, 350, 400, 500 and 750 ppm) were tested over a 62-hour period. Notwithstanding that the polymerization process for roughly all the above quantities initiated within 24 hours, yet during the first hour polymerization was observed only for the batch with the highest concentration (750 ppm). Similar batch tests employing pure silica solutions at pH 7 were also performed by Bremere et al. [20]. In this study, two extreme supersaturation levels were tested, namely 200 and 700 ppm. The outcome was a stable solution for the low supersaturation batch, in which monomeric silica dropped to merely 180 ppm after 30 hours, whereas rapid polymerization occurred for the high supersaturation batch already from the beginning of the run, in which silicic acid was declined to about 400 ppm after 2 hours. The above discussion reveals a tangible asset of CCRO over conventional RO during the treatment of supersaturated waters.Taking a targeted final silica concentration of 500 mg/L as an example, the difference between the two configurations in terms of scaling potential can be reflected. More specifically, the maximum time period that a membrane in a CCRO configuration would experience the highest supersaturation conditions would be less than one hour (it is noted that this is a quite conservative estimation since in practice the real time would be merely several minutes). As was shown from the previously presented results, this time is not sufficient for polymerization to initiate. On the other hand, the respective time period for the last membrane of a conventional RO system would be several days, thus monomeric silica would have been completely polymerized, which as will be discussed later is disadvantageous in terms of fouling propensity.

As far as hardness is concerned, it has a clear effect on silica scaling potential in either basic or neutral environment, yet to a totally different extent. As was shown, at high pH silicate anions reacted immediately with hardness ions forming metal-silicates as well as they were adsorbed on Mg^{2+}- and Ca^{2+} hydroxides. The formation of magnesium silicates at pH values above 8.5 has already been reported in various studies ([21], [39], [40]). This means, that in this case the depletion of monosilicic acid is not related to the polymerization process itself but to the monomeric silica co-precipitation with magnesium and calcium cations. Hence, the quantity of silica that was not detectable by the silicomolybdate method, had been removed from the solution as precipitate. On the contrary, at near

neutral pH conditions hardness cations do not react with monomeric, polymeric or colloidal silica. This was clear especially from the analyzed samples collected from the brines of the CCRO tests. It is reminded that there was no loss of magnesium in the brine, despite the substantially high concentration of both the SiO_2 and Mg^{2+} constituents and despite the fact that intense silica precipitation took place. Nonetheless, although hardness does not react with silica, its presence in the solution still enhances the risk of precipitation by accelerating the silica colloids agglomeration. Taking this into consideration, it can be deduced that the quantity of silicic acid that was 'lost' during the batch tests at pH 7, was not removed from the solution but it was transformed into a higher molecular weight silica form. The role of calcium and magnesium in promoting silica polymerization in neutral pH environments has also been established through carried out batch tests in the studies of Kempter et al. [4], Sheikholeslami and Tan [41] as well as Koo et al. [42]. However, contrary to the study of [41] where Mg^{2+} hardness exhibited greater effect as compared to Ca^{2+}, in the current study a similar effect between the two, if not greater of Ca^{2+}, was found.

Based on the previous discussed points, important conclusions about the best operation practices can be drawn, when it comes to RO operations treating silica-rich feed waters. Particularly, in the absence of hardness ions (e.g. due to their removal in an ion-exchange pre-treatment step) the most preferable option would be operating the system at high pH conditions (pH>10), so as to take advantage of silica's great solubility. This could be of special interest for facilities treating waters displaying already elevated pH values, in which cases the cost of further increasing the pH to the desired value would be restricted. Of course, care should be taken so that the upper pH admissible limits provided by the membrane manufacturers are not exceeded. On the other hand, when Mg^{2+} and/or Ca^{2+} cations are part of the feed, pH values below 8.5 should be applied in order to avoid the formation of insoluble metal silicates. Especially, lowering the pH below 6 could substantially slow down silica polymerization rate, owing to the widespread dominance of unionized monomeric units along with the limited presence of hydroxide anions, leading to prolonged induction times. According to Braun et al. [43], polymerization rate is comparatively rapid at pH values between 6.5 and 8.5, but it slows down significantly at pH 5.5.

5.2. Discussion on the CCRO filtration tests results

The obtained results revealed significant findings regarding the treatment of a saturated silica solution in the presence of magnesium hardness by means of a CCRO desalination system. The initial silica-rich composition (120 mg/L SiO_2) in conjunction with the Mg^{2+} (24 mg/L) existence rendered the synthetic feed solution particularly 'harsh' in terms of scaling potential, especially if the neutral pH conditions along with the non-usage of antiscalants are also taken into account. More specifically, throughout the entire CCD process the system operated continuously under supersaturated conditions, as silica ranged from 120 to 1320 mg/L, while at neutral pH silica solubility approaches its minimum value [21]. Despite those unfavourable conditions, a cumulative total operational duration of about 11 hours without scaling indications was achieved, during which a maximum recovery of 90.9% was accomplished. Presumably, at that point some colloidal deposits started to form and the membrane surface to be partially covered. Nonetheless, it was not until after additional 3 hours of operation that severe scaling evidently took place. Many studies ([40], [44], [43]) seem to converge to the inference that under highly supersaturated conditions the membrane clogging mechanism proceeds via an initial colloidal gel attachment onto the membrane surface followed by adsorption of monomeric units, as depicted in Figure 5.1 [44]. This deposition of monomers appears to cement the initially porous colloidal agglomerates and to transform them into a more compact layer in time [44]. The results of the present work seem to fully conform with the scientific consensus regarding the aforementioned fouling mechanism. This is because, as was discussed, the vast majority of total silica was polymerized, thus polymers precipitation should be responsible for the apparent permeability decline. Besides, the diminished monomers quantity measured in the sequences with scaling was the consequence of their attachment to the colloidal precipitates.

As was described in the theoretical part of this study (see 2.2.3), membrane clogging can be induced by either monomeric or polymeric deposition. What most of the researches suggest is that the key mechanism via which scaling in RO operations proceeds, comprises the polymeric deposition process [20] [43]. However, cases of membrane deposits believed to be caused by monomeric silica have been reported as well, such as the study of Semiat et al. [44], where scaling at low supersaturation conditions (after 20% recovery of an initially 150 ppm silica solution in the presence of high hardness

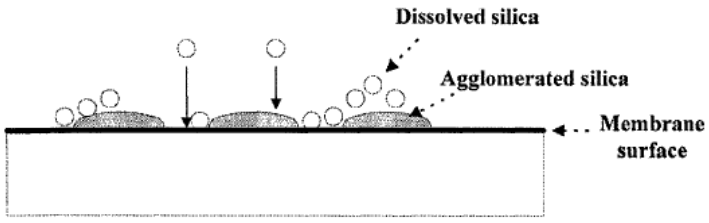

Figure 5.1: Silica deposition mechanism under highly supersaturated conditions [44].

concentration) was observed. The results emerged from the current study, especially after comparison with Motchan's results [15], constitute an essential verification of the widely accepted higher vulnerability of RO systems to colloidal than to monomeric scaling. More precisely, the maximum cumulative operational scaling-free duration, when polymers were predominant in the solution, was roughly 14 hours. On the other hand, in [15] it was shown that silica monomers with concentrations ranging from 120 mg/L to 1800 mg/L were effectively treated for a cumulative 26-hour CCD duration without scaling indications. Despite the obvious greater susceptibility of membrane desalination processes to polymeric than to monomeric silica fouling, more intensive research is required in order to define the boundaries of CCRO sytems resilience against monomeric scaling in the long run.

To the best of author's knowledge, an analogous research to the current pilot-scale study investigating the capability limits of a CCRO configuration to withstand silica scaling under considerably adverse conditions is not available in the relevant literature. In their experimental research, Gal et al. [13] employing a pilot CCRO setup treated municipal water (553 μS/cm) containing 32 ppm SiO_2 and 65 ppm Ca^{2+} among other constituents, up to a recovery grade of 96%. Hence, the maximum SiO_2 concentration measured in the loop was 800 ppm. Filtration sequences of a total cumulative operational duration of 24 hours were performed at constant 27.5 L/m^{2}h flux and at 20.7^{o}C, without any indication of fouling or scaling. It is pointed out that pH 5 was steadily maintained, whereas an antiscalant dedicated to silica was employed. A similar CCRO pilot test was realized by Sonera et al. [14], during which well-water was desalinated, containing among other ingredients 57 ppm SiO_2, 280 ppm Ca^{2+} and 5 ppm Mg^{2+}. Throughout the overall 8-hour trial, a maximum recovery of 93.8% was achieved, translating into a silica concentration of 919 ppm in the final brine. In this case a constant 17.2 L/m^{2}h flux was applied, while pH 5.5 was steadily kept and a suitable antiscalant was used. Although both the aforementioned studies demonstrated a promising propensity of CCRO against silica scaling, the contribution of the system configuration itself was only partially revealed, since in both cases its ability to endure high silica supersaturations was largely assisted by the low pH values as well as the antiscalant employment. That is to say, the pure effect of the CCRO configuration could not be isolated under the tested conditions. Therefore, it is hoped that the present work will further shed light on the actual capacity boundaries of CCRO configurations to resist and delay membrane damage caused by silica fouling.

Undoubtedly, an essential part of the ongoing research regarding CCRO comprises its direct comparison with conventional RO, both in overall terms as well as specifically in the field of silica scaling resistance potential. Focusing on the latter, the demonstration of experimental results referring to silica solutions treated by conventional RO is of special interest and it is sought here. Initially, a research [45] conducted at TU Delft examined the treatment of silica-rich solutions in the presence of high hardness concentration. More specifically, the feed solution, partly containing 300 ppm SiO_2, 250 ppm Ca^{2+} and 370 ppm Mg^{2+}, was treated by a single RO membrane element at constant flux of 15 L/m^{2}h for a 8-hour operational period. The solution temperature was 21.7^{o}C having a pH value of 6.8, while no antiscalants were used. The results revealed that an intense fouling process begun after approximately 3 hours of operation. What is more, various RO filtration experiments with supersaturated silica solutions were carried out in the context of Semiat et al. [44] study. In one of them, a feed solution composed of 150 ppm SiO_2, 2500 ppm Ca^{2+} and 800 ppm Mg^{2+} was processed by a RO system in a 7-hour run. According to the results, the onset of permeability decline equivalent to scaling occurrence was detected at about 20% of recovery grade, thus when the solution concentration was about 188 ppm SiO_2, 3125 ppm Ca^{2+} and 1000 ppm Mg^{2+}. Another trial concerned an initially highly supersaturated feed solution containing 600 ppm SiO_2, 400 ppm Ca^{2+} and 200 ppm Mg^{2+}. In this case, the feed composition was kept fixed, whereas the solution was treated by means of a RO membrane for 6 hours.

A rapid precipitation process was already evident during the first hour of operation, while after 6 hours the permeate flow was almost totally suppressed. This specific experiment was repeated under exactly the same conditions, with the only variation being the starting concentration of silica which dropped to half the initial value (300 ppm). In this case, a relatively prompt deposition process was also observed, yet in a much lower rate as compared with the previous trial. Especially, the rate of the permeability drop for the 300 ppm SiO_2 solution was roughly 5% per hour throughout the six experimental hours, whereas the respective permeability drop for the 600 ppm SiO_2 solution was approximately 65% during the first hour. All the previously presented conventional RO tests results conducted by [44] were realized in the absence of antiscalants. Kempter et al. [40] investigated membrane silica scaling from a different experimental perspective. In particular, they placed a piece of membrane into a stirred silica supersaturated solution inside a beaker examining silica adsorption on the membrane over time, by means of atomic force microscopy (AFM). The solution consisted of 510 ppm SiO_2, 160 ppm Ca^{2+} and 24 ppm Mg^{2+} dissolved in distilled water at pH 7, whereas the temperature was constantly kept at 40^{o}C. The membrane piece was studied at 1, 4 and 9 hours of operation. The first analysis after 1 hour revealed few spherical silica colloids with sizes between 20 and 30 nm attached to the membrane. The number of the attached silica colloids increased until the next membrane examination at 4 hours of operation, while at that time some clusters between the colloids were also observed. Finally, after 9 hours the membrane surface was entirely covered by colloidal agglomerates. In the light of the above discussion, it could be stated that the results demonstrated in the current work constitute solid experimental evidence of the superiority of semi-batch over continuous RO configurations in terms of silica fouling retardation. In particular, the CCRO system used in the present study treated a silica-rich feed solution for initially 3.3 hours (with SiO_2 ranging from 120 to 730 ppm and Mg^{2+} from 24 to 148 ppm) and subsequently for about 7.7 hours (with SiO_2 ranging from 120 to 1317 ppm and Mg^{2+} from 24 to 267 ppm) without any scaling manifestations, while it took another $\sim$3 hours for severe fouling to take place. Apparently, this performance surpasses the respective conventional RO capabilities, essentially confirming the CCRO greater efficacy with respect to silica scaling retardation.

Finally, as Gal et al. [13] remarked, a significant advantage of CCRO configurations which allows them to treat solutions displaying extreme supersaturations comprises the fact that those appear only for a restricted time frame towards the end of each sequence, before brine release takes place and be replaced by fresh feed normally occurring at sub-saturated conditions. This is especially the case, when the duration of supersaturation occurrence in the circulated solution is lower than the induction time of the sparingly soluble salts contained in the brine. Besides this, the outcome of the current research seems to expand the justification for the CCRO scaling resilience beyond the short-time operation effect. As was shown in the results section, the vast majority of total silica leaving the system was in polymeric form, thus silica induction time had been by far exceeded. In an attempt to quantitatively estimate the period during which silica polymers were present in the recirculated brine, it was assumed that nucleation begun at the moment when SiO_2 and Mg^{2+} concentrations were 600 ppm and 120 ppm, respectively. This assumption was based on the graph of Figure 4.7, which shows that under those conditions polymerization immediately initiates. In practice, this assumption underestimates the actual duration of polymers existence in the concentrate, since according to the same graph polymerization had already started from a lower supersaturation level, yet it is used here indicatively. Hence, according to the made assumption the required time for the aforementioned concentrations to be reached was about 15 min. This means, that the brine residence time in the loop exceeded silica induction time for at least 5 min in the 20 min sequences and for 25 min in the 40 min sequences. Taking the prevailing extreme supersaturation conditions (leading to promptly growing colloids) into consideration, it would be reasonably expected that this time should be sufficient for fouling to take place. Since for several consecutive sequences this was not the case, it is plausible to suspect that CCRO operational conditions themselves play a role in the obstruction of silica fouling. It is therefore hypothesized, that the non-steady conditions which are predominant during CCD processes effectively disturb colloids deposition and attachment to the membrane, as opposed to the steady-state conventional RO conditions. Those non-steady conditions essentially reflect the processes of the continuous mixing of the incoming feed with the recirculated stream as well as of the recurring dilution of the brine by the less concentrated fresh feed solution. Undoubtedly, more research is required to underpin the aforementioned hypothesis as well as to more thoroughly investigate the exact mechanisms governing the apparent enhanced fouling resilience exhibited by CCRO configurations.

5.3. Overall discussion

Membrane scaling induced by silica or silicates deposition has been long recognised as a notorious issue for desalination applications due to the irreversible damage it causes. Moreover, the complexity of silica chemistry in conjunction with its dependency on numerous and often unstable parameters render its behaviour highly unpredictable. Traditionally, the common strategy for controlling silica scaling in RO applications has been the following of the standard industry guideline, which constrains the maximum silica concentration in the brine to roughly 120 mg/L in the absence of antiscalants, while the respective limit increases to 300 mg/L when antiscalants have been employed [41]. However, this restriction may be particularly conservative in many cases leading to unnecessary water wastage or to excessive antiscalant usage. A major reason that RO facilities do not frequently deviate from those guidelines constitutes the lack of a simple, effective as well as inexpensive method to predict silica scaling potential.

The current study experimentally proved the higher tendency of CCRO configurations to resist and delay silica scaling in comparison to conventional RO. Nonetheless, the problem of silica scaling unpredictability still remains. Inspired by the experimental work as well as the results obtained from the present study, a simple customized method is suggested to evaluate silica scaling potential as well as to define safe operating limits of CCRO applications, before their actual implementation takes place. As was previously discussed, keeping silica in its monomeric form is beneficial in terms of controlling silica fouling. It is therefore suggested that through simple batch tests (similar to those carried out in this research) simulating actual brines, silica state under any given conditions could be monitored throughout the entire simulated CCRO process. Based on the results, the decision could be made whether scaling in the specific application is probable or not. More explicitly, a synthetic solution representing the actual final brine after the desired recovery has been achieved should be first prepared. This would involve the simulation of the exact pH, temperature and final brine composition. By analysing samples taken from the stirring batch periodically via the silicomolybdate method, the state of silica at any given moment could be easily verified. If the monomeric quantity would remain contant for the entire examined time frame, this would imply the absence of polymers and consequently a safe CCRO operation. On the other hand, reduced monomeric silica quantity would indicate colloids formation and thus an increased scaling potential. In addition, different operating factors, water types and appropriate antiscalant quantities could be tested in simple 1-hour batch trials, creating a safe operation profile and allowing for the optimization of each individual application. Apparently, the power of such a method is related to its simplicity, affordability, short duration as well as its versatility, since virtually any customized conditions can be readily simulated and tested. It is hoped, that such a method would further promote the overall optimization of CCRO operations towards more efficient and sustainable desalination processes.

6

Conclusions

The results of the batch tests carried out without pH adjustment (pH>10) showed that no significant polymerization in the pure silica solutions took place, even at roughly 10 fold supersaturation level (1180 mg/L SiO_2). The apparent great silicic acid stability was due to the the high solubility of silica at highly alkaline conditions. However, in the presence of hardness ions insoluble Mg^{2+}- and Ca^{2+} silicates formed instantaneously. In the batches with pure silica solutions at pH 7, no important polymerization was observed up to about 3.8 fold supersaturation level (~450 mg/L) for the 4-hour experimental duration. Nonetheless, at higher supersaturations polymerization begun within this time frame. Hardness cations present in neutral pH solutions effectively accelerated silica polymerization process, yet without reacting with either monomeric or polymeric silica. Based on those findings, the optimal conditions regarding RO applications treating waters containing silica were determined. For silica solutions in the absence of hardness ions, pH conditions higher than 10 constitute the safest option. On the contrary, in the presence of Mg^{2+} and/or Ca^{2+} low pH should be applied, especially below 6 in which case polymerization rate slows down significantly.

The CCRO filtration experiments resulted in a total cumulative CCD operation time of about 14 hours before severe scaling occurred. Throughout the consecutive scaling-free sequences SiO_2 in the loop ranged from 120 to 1316 mg/L, translating into a maximum recovery of 90.9%. Soluble silica measurements in the final brine of each CCD sequence showed that important polymerization took place in all cases during the recirculation process, whereas IC analysis confirmed that Mg^{2+} ions were not part of the formed scale. It was concluded that Mg^{2+} effectively promoted silica polymerization, which is in total agreement with the results acquired from the batch tests.

The comparison between the results obtained in the current work with results from other studies taken from the literature revealed the greater tendency of CCRO to effectively delay silica scaling as compared to conventional RO. In addition to the common justification for the CCRO higher performance, referring to the much shorter time frames that highly supersaturated conditions occur in CCRO than in conventional RO configurations, it was hypothesized that the prevailing non-steady conditions (continuous mixing and dilution of the circulated brine by the incoming fresh feed) partially contribute to the better CCRO performance. Moreover, it was deduced that silica scaling observed during the current filtration tests, proceeded via a mechanism involving the initial adherence of colloidal polymers to the membrane surface followed by silica monomeric units adsorption onto them, making the scale layer harder over time.

Finally, a simple method was proposed by the author aiming at the study of silica state inside the CCRO loop under any given operating conditions, before the actual filtration process would be performed. This could be particularly useful in order to predict the scaling potential as well as to identify the optimal operating conditions that would ensure the remaining of silica in its monomeric form, which as was shown greatly reduces the risk of scaling.

7

Recommendations

In the present study the greater intrinsic propensity of CCRO to delay silica fouling in comparison with conventional RO was shown. It is hoped, that this promising outcome will trigger efforts for further investigations targeting at the optimization of CCRO operations for more effective silica scale control. To that end, some recommendations for future research are proposed on the basis of the findings arisen from the current work. Those recommendations concern both practical optimization modifications as well as more scientific research aspects regarding CCRO.

- The validation of CCRO superiority over RO in terms of silica scaling retardation was based on the comparison with results from other studies. Although this enabled a solid conclusion to be drawn, this was mostly qualitative, since various parameters that could have an effect on the fouling process were different among the compared tests. Aiming at a more quantitative assessment of the two contrasted configurations, a continuous RO filtration test using a single membrane module is proposed under identical operating conditions with those employed in the current CCRO tests. These would include the same flux, pH, temperature as well as feed flow rate (ensuring identical cross-flow velocity). Additionally, the last membrane element of a conventional christmas tree configuration should be simulated, when the same high recovery as in the current tests is achieved. This specific element is the most vulnerable to scaling. Hence, the composition of the solution serving as feed should be that of the original solution but adequately concentrated to simulate the final brine. The filtration process should be continuous and the potential scaling occurrence should be monitored. In that way the straightforward quantitative comparison between CCRO and RO would be enabled, in terms of silica scaling retardation efficacy.

- The filtration tests of the present study were realized under unfavorable operating conditions in relation to the fouling tendency. In future research, focus should be given on the CCRO performance limits under milder (and more practical) conditions. In particular, pH could play an important role in further mitigation of silica scaling. For instance, pH values lower than 6 could be applied, because acidic conditions are expected to considerably slow down the silica polymerization rate. This would be of special interest when silica solutions containing hardness ions are treated.

- The developed fouling in the current CCRO tests proceeded via a mechanism involving an initial deposition of colloidal polymers onto the membrane surface followed by monomeric units adsorption, which made the scale layer harder over time. The deduction about this clogging mechanism was drawn indirectly, by means of silica and magnesium concentration measurements in combination with bibliographic references. The scale itself was not analysed. In general, the exact mechanism of colloids attachment on membranes is not totally understood yet and in that sense its extensive research remains an intriguing topic. Therefore, scale analysis (e.g. by means of AFM) in future filtration tests is suggested, in order to shed light on the colloids attachment mechanism as well as on the sizes of the precipitated agglomerates.

- In Section 5.3, a method was proposed that enables the study and prediction of the conditions under which silica in the CCRO recirculation loop would remain in its monomeric state, throughout the entire filtration process. Undoubtedly, the prevention of silica polymerization comprises a crucial step towards silica scaling mitigation. Nevertheless, as it has already been mentioned, scaling initiated by monomers deposition could also occur, although less frequently. It is, therefore, essential to assess the effectiveness and if possible to determine the limits of CCRO to retard or even to prevent scaling caused by silicic acid. The successful short-term performance of CCRO was validated by Motchan's experiments [15]. However, it is crucial to evaluate the long-term performance as well, which is important for practical applications. Furthermore, since monomeric silica scaling is principally influenced by the concentration polarization (CP) boundary layer, it is proposed to apply a cross-flow velocity as high as possible, which would effectively counteract the detrimental effects of CP. It is reminded, that CCRO allows for easy adjustment of the cross-flow velocity irrespective of the resulted flux as well as the final selected recovery.

- In Section 5.2, the hypothesis was made that the non-steady conditions of the CCRO process (constant mixing and dilution of the brine) contribute to the scaling retardation. Throughout the 40 min CCD sequences performed in the current study, SiO_2 concentration in the recirculated stream was gradually increased from 120 up to roughly 1280 mg/L, under continuous dilution and mixing with the incoming fresh feed. At half the operation time (20 min), the respective concentration values were $\sim$750 mg/L SiO_2 and $\sim$150 mg/L Mg^{2+}. In order to validate the above hypothesis a similar to the CCRO trials test is proposed as follows. The new feed solution should be composed of 750 mg/L SiO_2 and 150 mg/L Mg^{2+}. Successive filtration runs of 40 min duration in PFD mode should be carried out, thus operating as conventional RO (without brine recirculation). However, at the end of every 40-min period flushing with low salinity water should be performed in order to eliminate the influence of stagnant zones experiencing permanently high supersaturations (in this case 750 mg/L). Thus, the filtration test would be conducted in 'batches' of PFD sequences treating highly saline water under steady conditions with regular intermediate flushing periods (PFD sequences with low salinity water) of few minutes. The flux and the cross-flow velocity should be identical with those of the original CCRO test. Throughout the consecutive 40 min PFD sequences, scaling monitoring should be realized by means of the MTC recording. Finally, the obtained scaling results could be contrasted with the ones emerged from the present study in order to evaluate the potential contribution of the non-steady conditions to scaling retardation.

Bibliography

[1] Ronan K McGovern et al. “On the potential of forward osmosis to energetically outperform reverse osmosis desalination”. In: *Journal of Membrane Science* 469 (2014), pp. 245–250.

[2] Lilian Malaeb and George M Ayoub. “Reverse osmosis technology for water treatment: state of the art review”. In: *Desalination* 267.1 (2011), pp. 1–8.

[3] Lauren F Greenlee et al. “Reverse osmosis desalination: water sources, technology, and today’s challenges”. In: *Water research* 43.9 (2009), pp. 2317–2348.

[4] A Kempter et al. “Controlling silica in water treatment applications”. In: *Kempter, T. Gaedt, V. Boyko, S. Nied, M. Kley, K. Huber//The International Desalination Association World Congress on Desalination and Water Reuse*. 2013.

[5] Elimelech M Phillip WA. “The future of seawater desalination: Energy, technology, and the environment Science 333712. Elimelech, M., and Phillip, WA (2011). The future of seawater desalination: Energy, technology, and the environment”. In: *Science* 333 (2011), p. 712.

[6] Jay R Werber, Akshay Deshmukh, and Menachem Elimelech. “The critical need for increased selectivity, not increased water permeability, for desalination membranes”. In: *Environmental Science & Technology Letters* 3.4 (2016), pp. 112–120.

[7] Cui Liu, Ken Rainwater, and Lianfa Song. “Energy analysis and efficiency assessment of reverse osmosis desalination process”. In: *Desalination* 276.1-3 (2011), pp. 352–358.

[8] Avi Efraty. “CCD series no-16: opened vs. closed circuit SWRO batch desalination for volume reduction of Silica containing effluents under super-saturation conditions”. In: *Desalination and Water Treatment* 57.21 (2016), pp. 9569–9584.

[9] David M Warsinger et al. “Energy efficiency of batch and semi-batch (CCRO) reverse osmosis desalination”. In: *Water research* 106 (2016), pp. 272–282.

[10] Jay R Werber, Akshay Deshmukh, and Menachem Elimelech. “Can batch or semi-batch processes save energy in reverse-osmosis desalination?” In: *Desalination* 402 (2017), pp. 109–122.

[11] Tianyu Qiu and Philip A Davies. “Comparison of configurations for high-recovery inland desalination systems”. In: *Water* 4.3 (2012), pp. 690–706.

[12] Richard L Stover. “Industrial and brackish water treatment with closed circuit reverse osmosis”. In: *Desalination and Water Treatment* 51.4-6 (2013), pp. 1124–1130.

[13] Z Gal et al. “CCD series no-20: high-flux low-energy upgrade of municipal water supplies with 96% recovery for boiler-feed and related applications”. In: *Desalination and Water Treatment* 57.43 (2016), pp. 20219–20227.

[14] V Sonera, J Septon, and Avi Efraty. “CCD series no-21: illustration of high recovery (93.8%) of a silica containing (57 ppm) source by a powerful technology of volume reduction prospects”. In: *Desalination and Water Treatment* 57.43 (2016), pp. 20228–20236.

[15] Thayn Malar Motchan. *Silica Scaling in Closed-Circuit Desalination*. 2019.

[16] H2O Engineering Inc. *Closed-Circuit Reverse Osmosis (CCRO)*. URL: `https://www.h2oengineering.com/technologies/closed-circuit-reverse-osmosis-ccro/`. (accessed: 28.04.2020).

[17] Desalitech. *Industrial Closed Circuit Reverse Osmosis Systems*. URL: `https://www.desalitech.com/industrial-closed-circuit-reverse-osmosis-systems/`. (accessed: 29.03.2020).

[18] Avi Efraty. “CCD series no-19: The lowest energy prospects for SWRO through single-element modules under plug-flow and closed-circuit desalination conditions”. In: *Desalination and Water Treatment* 57.46 (2016), pp. 21696–21711.

[19] Robert Y Ning, Anthony J Tarquin, and John E Balliew. “Seawater RO treatment of RO concentrate to extreme silica concentrations”. In: *Desalination and water treatment* 22.1-3 (2010), pp. 286–291.

[20] Ingrida Bremere et al. “Prevention of silica scale in membrane systems: removal of monomer and polymer silica”. In: *Desalination* 132.1-3 (2000), pp. 89–100.

[21] Nicholas A Milne et al. “Chemistry of silica scale mitigation for RO desalination with particular reference to remote operations”. In: *Water research* 65 (2014), pp. 107–133.

[22] Robert Y Ning. “Discussion of silica speciation, fouling, control and maximum reduction”. In: *Desalination* 151.1 (2003), pp. 67–73.

[23] R Sheikholeslami et al. “Some aspects of silica polymerization and fouling and its pretreatment by sodium aluminate, lime and soda ash”. In: *Desalination* 150.1 (2002), pp. 85–92.

[24] Richard N. Palmer, ed. *World Environmental and Water Resources Congress 2010: Challenges of Change*. World Environmental and Water Resources Congress 2010. The address of the publisher: American Society of Civil Engineers, May 2010.

[25] Robert Y Ning. “Reactive silica in natural waters—A review”. In: *Desalination and water treatment* 21.1-3 (2010), pp. 79–86.

[26] Ralph K Iler. “The Chemistry of Silica John Wiley & Sons”. In: *New York* (1979), pp. 30–62.

[27] William L Marshall and Chen-Tung A Chen. “Amorphous silica solubilities V. Predictions of solubility behavior in aqueous mixed electrolyte solutions to 300 C”. In: *Geochimica et Cosmochimica Acta* 46.2 (1982), pp. 289–291.

[28] Akira Ueda et al. “Silica removal from Mokai, New Zealand, geothermal brine by treatment with lime and a cationic precipitant”. In: *Geothermics* 32.1 (2003), pp. 47–61.

[29] Mai Saadi. “The Root of Silica Scale Formation and Its Remedy”. In: *Global Journal of Engineering Sciences* 3 (Oct. 2019). DOI: 10.33552/GJES.2019.03.000565.

[30] Zahid Amjad. *Mineral scales in biological and industrial systems*. CRC Press, 2013.

[31] CAC Van de Lisdonk et al. “Prediction of supersaturation and monitoring of scaling in reverse osmosis and nanofiltration membrane systems”. In: *Desalination* 138.1-3 (2001), pp. 259–270.

[32] Saqib Shirazi, Che-Jen Lin, and Dong Chen. “Inorganic fouling of pressure-driven membrane processes—a critical review”. In: *Desalination* 250.1 (2010), pp. 236–248.

[33] SGJ Heijman et al. “Application of ScaleGuard® at reverse osmosis and nanofiltration installations”. In: *Water Science and Technology: Water Supply* 3.5-6 (2003), pp. 133–138.

[34] Ran Shang et al. “Atmospheric pressure atomic layer deposition for tight ceramic nanofiltration membranes: synthesis and application in water purification”. In: *Journal of Membrane Science* 528 (2017), pp. 163–170.

[35] Dionysia Diamantidou. *Ionic separation of the IEX spent regenerant using Nanofiltration*. 2018.

[36] *Du Pont Technical Information Manual.* 1980.

[37] *Soluble Silicate for Water Control Lost Circulation*. 2006.

[38] NI Nesterchuk and TA Makarova. “The formation of aqueous magnesium silicate in the interaction of solutions of magnesium chloride and sodium metasilicate”. In: *Bulletin of the Academy of Sciences of the USSR, Division of chemical science* 19.10 (1970), pp. 2053–2055.

[39] Douglas B Kent and Miriam Kastner. “Mg2+ removal in the system Mg2+—amorphous SiO2—H2O by adsorption and Mg-hydroxysilicate precipitation”. In: *Geochimica et Cosmochimica Acta* 49.5 (1985), pp. 1123–1136.

[40] Andreas Kempter et al. “New insights into silica scaling on RO-membranes”. In: *Desalination and Water Treatment* 51.4-6 (2013), pp. 899–907.

[41] R Sheikholeslami and S Tan. “Effects of water quality on silica fouling of desalination plants”. In: *Desalination* 126.1-3 (1999), pp. 267–280.

[42] T Koo, YJ Lee, and R Sheikholeslami. “Silica fouling and cleaning of reverse osmosis membranes”. In: *Desalination* 139.1-3 (2001), pp. 43–56.

[43] Gerd Braun et al. “Investigations of silica scaling on reverse osmosis membranes”. In: *Desalination* 250.3 (2010), pp. 982–984.

[44] Raphael Semiat, Iris Sutzkover, and David Hasson. “Scaling of RO membranes from silica supersaturated solutions”. In: *Desalination* 157.1-3 (2003), pp. 169–191.

[45] AH Haidari. “High silica concentration in RO concentrate and Magnesiumsilica polymers formation”. In: (2011).

A

Composition of the batch solutions

Table A.1: Overview of the conducted batch tests. The values shown in the table represent the final concentrations of SiO_2 (theoretical initial value 70 or 120 mg/L), Mg^{2+} (theoretical initial value 24 mg/L) and Ca^{2+} (theoretical initial value 40 mg/L) used in the prepared batches after the indicated recovery (R) had been achieved.

Theoretical initial concentration	**80% R**	**85% R**	**90% R**
SiO_2 (70 mg/L)	350 mg/L	460 mg/L	-
+ *Mg*	120 mg/L	160 mg/L	-
+ *Ca*	195 mg/L	260 mg/L	-
+ *Ca/Mg*	195/120 mg/L	260/160 mg/L	-
SiO_2 (120 mg/L)	600 mg/L	790 mg/L	1180 mg/L
+ *Mg*	120 mg/L	-	-
+ *Ca*	195 mg/L	-	-
+ *Ca/Mg*	-	-	-

B

Membrane specification data sheet

FILMTEC™ Fiberglassed Elements for Light Industrial Systems

Description

FILMTEC™ brackish water reverse osmosis membrane elements provide consistent system performance in light industrial applications.

- FILMTEC™ BW30-4040 is an industry standard for reliable operation and production of high quality water.
- FILMTEC™ BW30-2540 elements are designed for systems smaller than 1 gpm (0.2 m^3/h) offering a hard shell exterior for extra strength.

Elements with a hard shell exterior are recommended for systems with multiple-element housings containing three or more membranes, as they are designed to withstand higher pressure drops.

Product Type

Spiral-wound element with polyamide thin-film composite membrane

Typical Properties

Product	Part Number	Feed Spacer Thickness (mil)	Permeate Flow Rate gpd (m^3/d)	Stabilized Salt Rejection %
BW30-4040	80783	34	2,400 (9.1)	99.5
BW30-2540	80766	28	1,000 (3.8)	99.5

1. Permeate flow and salt rejection based on the following test conditions: 2,000 ppm NaCl and 225 psig (15.5 bar), pH 8, 77°F (25°C) and 15% recovery.
2. Minimum salt rejection is 98.0%.
3. Permeate flows for individual elements may vary +/-20%.

Element Dimensions

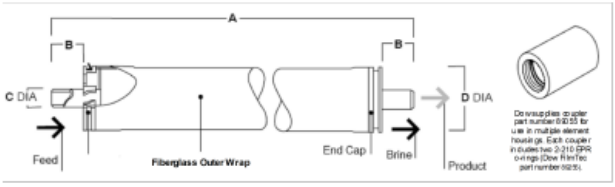

Dimensions – inches (mm)				1 inch = 25.4 mm
Product	A	B	C	D
BW30-4040	40.0 (1,016)	1.05 (26.7)	0.75 (19)	3.9 (99)
BW30-2540	40.0 (1,016)	1.19 (30.2)	0.75 (19)	2.4 (61)

1. Refer to FilmTec Design Guidelines for multiple-element systems.
2. BW30-2540 elements fit nominal 2.5-inch I.D. pressure vessel. BW30-4040 elements fit nominal 4-inch I.D. pressure vessel

Figure B.1: Specification data sheet of the BW30-4040 membrane element used in the experimental process.

C

Composition of the CCRO feed solutions

The constituents of interest for the conducted CCRO filtration tests were SiO_2 and Mg^{2+}. However, since sodium metasilicate and magnesium chloride were the reagents used for creation of the desired solutions as well as hydrochloric acid and sodium hydroxide solutions were employed for the pH regulation, some Na^+ and Cl^- ions were also present in the prepared solutions. Table C.1 presents the exact synthetic feed solutions composition.

Table C.1: The exact composition of the prepared feed solutions employed in the performed CCRO filtration experiments.

Element	Concentration
SiO_2	120 mg/L
Mg^{2+}	24 mg/L
Na^+	92 mg/L
Cl^-	249 mg/L

D

Original graph from literature

Part of the batch tests results presented in the following graph were used in Figure 4.6. More specifically, the soluble silica concentration changes over the first 4 hours were used. The present original graph was received from [4].

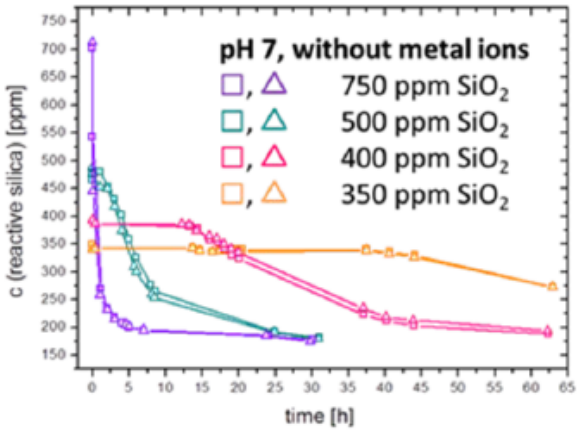

Figure D.1: Soluble silica concentration variation over time in the absence of hardness ions at pH 7. The graph was received from [4].

E

Silica mass balance graphs

E.1. SiO_2 mass balance for the 20 min sequences 6-10

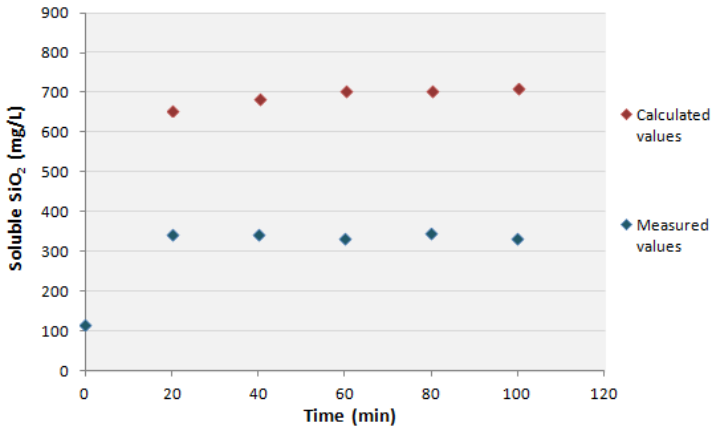

Figure E.1: Measured and calculated soluble SiO_2 concentration values in the final brine of each 20 min sequence. The depicted values concern sequences 6 - 10.

E.2. SiO_2 mass balance for the 40 min sequences 1-5

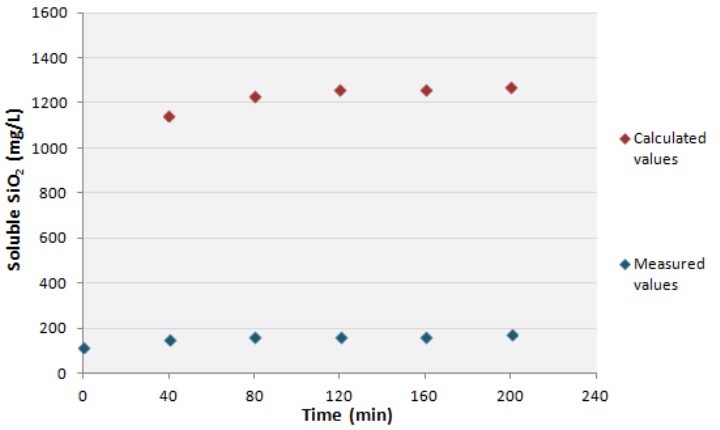

Figure E.2: Measured and calculated soluble SiO_2 concentration values in the final brine of each 40 min sequence. The depicted values concern sequences 1 - 5.

E.3. SiO_2 mass balance for the 40 min sequences 11-15

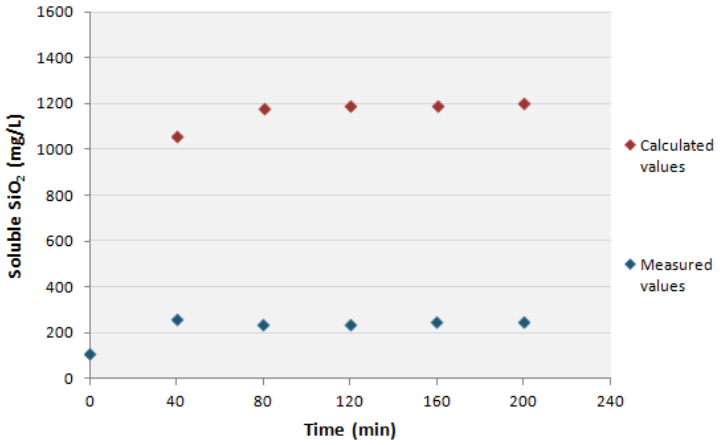

Figure E.3: Measured and calculated soluble SiO_2 concentration values in the final brine of each 40 min sequence. The depicted values concern sequences 11 - 15.

E.4. SiO_2 mass balance for the 40 min sequences 21-25

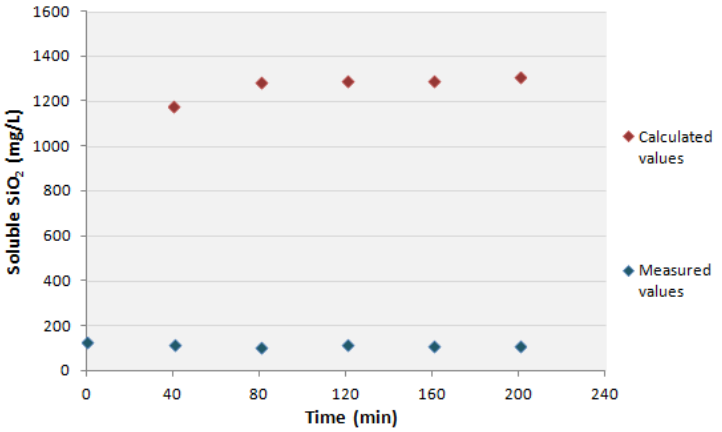

Figure E.4: Measured and calculated soluble SiO_2 concentration values in the final brine of each 40 min sequence. The depicted values concern sequences 21 - 25.

E.5. SiO_2 mass balance for the 40 min sequences 26-30

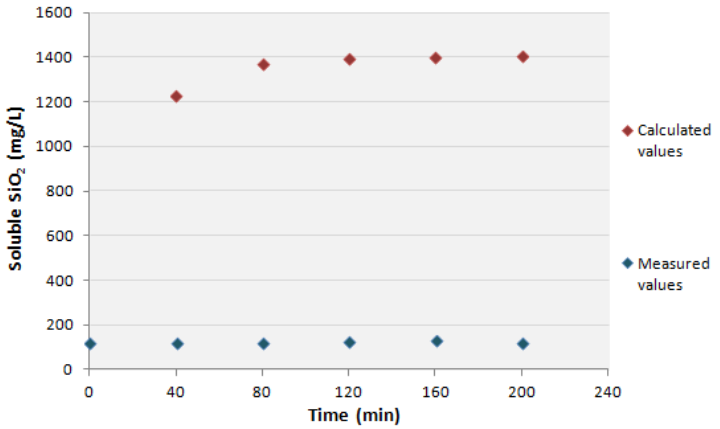

Figure E.5: Measured and calculated soluble SiO_2 concentration values in the final brine of each 40 min sequence. The depicted values concern sequences 26 - 30, which were conducted in the absence of Mg^{2+}.

E.6. Mg^{2+} mass balance for the 40 min sequences 16-20

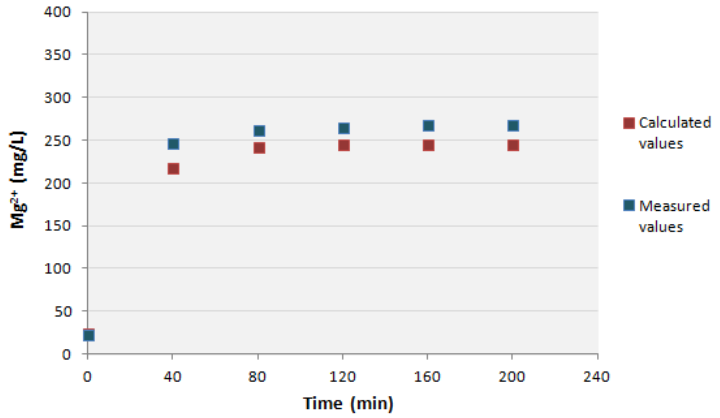

Figure E.6: Measured and calculated Mg^{2+} concentration values in the final brine of each 40 min sequence. The depicted values concern sequences 16 - 20.